A re-investigation of hummocky moraine formed from ice sheet decay using geomorphological and sedimentological evidence in the Vomb area, southern Sweden

Tim Bjermo

Dissertations in Geology at Lund University,
Master's thesis, no 643
(45 hp/ECTS credits)

Department of Geology
Lund University
2022

A re-investigation of hummocky moraine formed from ice sheet decay using geomorphological and sedimentological evidence in the Vomb area, southern Sweden

Master's thesis
Tim Bjermo

Department of Geology
Lund University
2022

Contents

Cover Picture: Deformation structures in glaciolacustrine sand.

TIM BJERMO

A re-investigation of hummocky moraine formed from ice sheet decay using geomorphological and sedimentological evidence in the Vomb area, southern Sweden

Tim Bjermo

Bjermo, T., 2022: A re-investigation of hummocky moraine formed from ice sheet decay using geomorphological and sedimentological evidence in the Vomb area, southern Sweden. *Dissertations in Geology at Lund University*, No. 643, 32 pp. 45 hp (45 ECTS credits).

Abstract: Glacial sediment-landform assemblages have long been used to reconstruct the dynamics of ice sheets throughout the Quaternary time period, particularly so for the period of the last glaciation in northern Europe and southern Scandinavia. One such sediment-landform assemblage is hummocky moraine, which has previously been used as an all-encompassing descriptive terminology strongly associated with dead ice meltout and passive deglaciation. The broad use of this terminology can often result in an incorrect classification of the landscape, which with its strong association to dead ice meltout results in a strong bias toward related deglaciation models.

A detailed remote- and field study was conducted over a region in Scania, southern Sweden, that has previously been classified as hummocky moraine. By remotely mapping individual hummocks and landforms on a large scale through the use of LiDAR data, the spatial components related to the hummocks were analysed and showed spatial order and clear orientations in the landscape. Two hummocks were examined and found to contain sedimentological evidence linked to an active ice-margin. With the addition of several ice-walled lake plains, it was concluded that the 'hummocky moraine' in the study area were formed from processes linked to both active and stagnant ice.

Keywords: glacial geomorphology, remote sensing, LiDAR, sedimentology, glacitectonite, deformation structures, hummocky moraine, quaternary geology, deglaciation.

Supervisor(s): Dr. Sven Lukas

Subject: Quaternary Geology

Tim Bjermo, Department of Geology, Lund University, Sölvegatan 12, SE-223 62 Lund, Sweden.
E-mail: ti0743bj-s@student.lu.se / timbjermo90@hotmail.com

En nyutredning av ett dödislandskap genom geomorfologiska och sedimentologiska observationer i Vombsänkan, södra Sverige

Tim Bjermo

Bjermo, T., 2022: En nyutredning av ett dödislandskap genom geomorfologiska och sedimentologiska observationer i Vombsänkan, södra Sverige. *Examensarbeten i geologi vid Lunds universitet*, Nr. 643, 32 sid. 45 hp.

Abstract: Glaciala sediment- och landformskonstellationer har länge använts för att rekonstruera inlandsisens dynamik och rörelser under Kvartärperioden, specifikt så för den senaste glaciationen i norra Europa och södra Skandinavien. En sådan sediment- och landformskonstellation är 'småkullig morän', som tidigare har använts som en övergripande och beskrivande term starkt associerad med dödisutsmältning och passiv deglaciation. Det breda användandet av sådan terminologi kan resultera i en inkorrekt klassifikation vid landskapskartläggning, som med sin starka association till dödisutsmältning resulterar i en bias till sådana associerade deglaciationsmodeller.

En detaljerad fjärr- och fältstudie genomfördes i en region i Skåne, södra Sverige, som tidigare kartlagts och klassificerats som ett småkulligt moränlandskap. Genom att digitalt kartlägga individuella kullar och landformer över ett stort område genom att utgå från LiDAR-data, så har den rumsliga komponent relaterad till kullarna analyserats och påvisade klara trender och riktningar i landskapet. Två kullar undersöktes närmare och påvisade sedimentologiska bevis som länkas till en aktiv israndtillhörande inlandsisen. Tillsammans med närvaron av flertalet lerplatåer så dras slutsatsen att landskapet är avsatt och format av processer länkade till en periodvis både aktiv och passiv inlandsis.

Keywords: glacial geomorfologi, fjärranalys, LiDAR, sedimentologi, glacitektonit, deformationstrukturer, småkullig morän, backlandskap, moränlandskap, kvartärgeologi, deglaciation.

Supervisor(s): Dr. Sven Lukas

Subject: Kvartärgeologi

Tim Bjermo, Geologiska institutionen, Lund Universitet, Sölvegatan 12, SE-223 62 Lund, Sverige.
E-post: ti0743bj-s@student.lu.se / timbjermo90@hotmail.com

1 Introduction

1.1 Background

Glacial sediment-landform assemblages have long been used to reconstruct the dynamics of ice sheets throughout the Quaternary time period (Hughes et al. 2016), particularly so for the period of the last glaciation in northern Europe and southern Scandinavia (Stroeven et al. 2016). A sediment-landform assemblage that is widespread but has unfortunately not received much research attention recently is the so-called hummocky moraine. Hummocky moraine has historically been associated with ice sheet stagnation and dead ice meltout, depositing *in situ* sediments into a chaotic and unorganized landform assemblage (Hoppe 1952; Gravenor & Kupsch 1959; Aario 1977). However, later regional studies and re-investigations of landscapes previously designated as hummocky moraine have instead shown hummocks and crestlines displaying a spatial order reminiscent of paleo ice-margins that track individual, inset retreat positions (Benn 1992; Bennett & Boulton 1993; Benn & Lukas 2006). Due to the spatial order and preservation of the hummocks as well as their sedimentological content, it could be demonstrated that they formed during the retreat of an active ice-margin, and therefore would be better re-classified as recessional moraines as the term hummocky moraine is too encompassing (Benn 1992; Bennett & Boulton 1993; Lukas 2003; Benn & Lukas 2006; Benn & Evans 2010).

In southern Sweden, this sediment-landform assemblage occurs in numerous places (Daniel 1992; Möller 2010; Peterson et al. 2017). The area south of the fault valley Fyledalen in Scania (Swe: Skåne), located in the northwestern Vomb depression (Swe: Vombsänkan), was mapped and described between the years 1985–1992 by SGU as part of a map series and associated map descriptions (SGU 1985; Daniel 1986; SGU 1989; Daniel 1992). The landscape has previously to a large extent been described as a hummocky dead ice landscape without any clear trends in the topography (Nelson 1949; Daniel 1986). The ridges, depressions, and other landforms are described as randomly oriented and interpreted to have formed from downwasting, around stagnant or dead ice, and melt out till.

Our knowledge regarding Quaternary deposits and landforms has dramatically changed since previous mapping through the widespread use of modern analogues and the availability of high-resolution imagery such as LiDAR (Light Detection And Ranging). This results in many landforms and landscape trends, the existence of which was at the time of previous mapping unrecognised, therefore being absent from the SGU map archives. SGU is continuously remapping areas to amend such issues, which might potentially result in a complete reinterpretation in the genesis of regional landscape development.

A recent look at a digital elevation model (DEM) constructed by modern LiDAR data (Lantmäteriet 2020) reveals a view of the topography that has been unavailable to previous mappers. Landforms hidden under forest in previously-used orthophotos become distinguishable when subjected to LiDAR and reveal geomorphological trends in the landscape that has previously been discarded as a randomly-oriented dead ice landscape. These new data open up the possibility of more detailed mapping and might thus necessitate a fresh inventory of the glacial geological components of the landscape leading to potentially new interpretations of how the landscape might have formed. There is much to be gained from systematically reinvestigating areas that have not been looked at or reviewed since the addition of ground-breaking methodological advances in current and following shifts in paradigms (Benn 1992; Chandler et al. 2018).

1.2 Aims

By identifying landform orientation trends in the landscape and by mapping the associated landforms through remote sensing data analysis, the author aims to reveal clues of the genesis of the landforms that has previously been described as a hummocky dead ice landscape (Daniel 1986; SGU 1989). The aims of this project are therefore:

(A) to establish the types and distribution of glacial and associated sediment-landform assemblages in the study area

(B) to reconstruct the processes of how the resulting landscape in the study area formed

(C) to shed light on ice dynamics during the deglaciation in the study area.

2 Study area and geological setting

The northwestern Vomb depression is located in the central part of the province of Scania in southern Sweden, with a study area of ca. 80 km^2 (Fig. 1). Much of this area had previously been classified as mainly hummocky moraine (Daniel 1986, 1992). This region encompasses, and is limited by, the fault valley to the south. Therein lies a focus-area of roughly 35 km^2

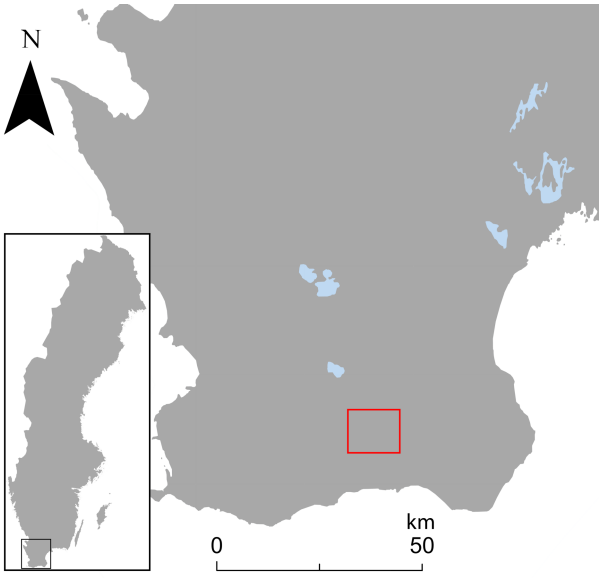

Figure 1. Map of Scania in southern Sweden with the study area (approximately 80 km2) highlighted in red.

(Fig. 2) subjected to detailed mapping within this report. The focus area is centred on and around the two lakes Sövdesjön and Snogeholmssjön.

2.1 Pre-Quaternary geological overview

The northwestern Vomb depression is part of a horst and graben system consisting of the fault valley Fyledalen in the northeast and the Romeleåsen horst in the southwest (Fig. 2) (Lindström et al. 2011). The horst und graben system originates from the Sorgenfrei-Tornquist Zone that spans the entire width of Scania in a northwest to southeast direction (Erlström et al. 2004; Lindström et al. 2011). The underlying crystalline basement is of Precambrian origin and part of the Baltic Shield, consisting mainly of granitic and granodioritic gneiss (Daniel 1992; Erlström et al. 2004; SGU 2005; Lindström et al. 2011). The crystalline bedrock can be found exposed in the southwest of the study area due to the uplift of the horst. The crystalline basement is riddled with intrusive diabase dykes that predate the sedimentary bedrock and display a northwest to southeast orientation along the Sorgenfrei-Tornquist Zone (Daniel 1992; Erlström et al. 2004; SGU 2005; Lindström et al. 2011).

The northwestern Vomb depression itself is mainly underlain by Mesozoic sediments and sedimentary bedrock that are covered by Quaternary deposits. These include, but are not limited to, mudstone, marlstone, siltstone, sandstone and limestone, all of varying compositions, including the corresponding sediments in lithified and non-lithified states (Daniel 1992; Erlström et al. 2004; Lindström et al. 2011).

2.2 Deglaciation of the Fennoscandian Ice Sheet

During the Quaternary time period covering the past 2.58 million years (Cohen & Gibbard 2019), Fennoscandia has been subjected to several glacial periods. The Weichselian glacial period is the last glacial period in Europe and spanned the period between 115 to 11.7 ka (Anjar 2012). A single glacial period does not necessarily indicate a single glacial advance followed by retreat, but can represent several colder stadials and warmer interstadials with the ice sheet reacting accordingly (Anjar 2012). Even within the timeframe of a stadial or interstadial, the ice masses of an ice sheet are known to fluctuate greatly. Decadal fluctuations are not uncommon, and there can even be noteworthy annual re-advances of the ice masses taking place (Benn & Evans 2010; Anjar 2012). At the point in time when the last glacial maximum (LGM) of the Fennoscandian Ice Sheet (FIS) occurred,

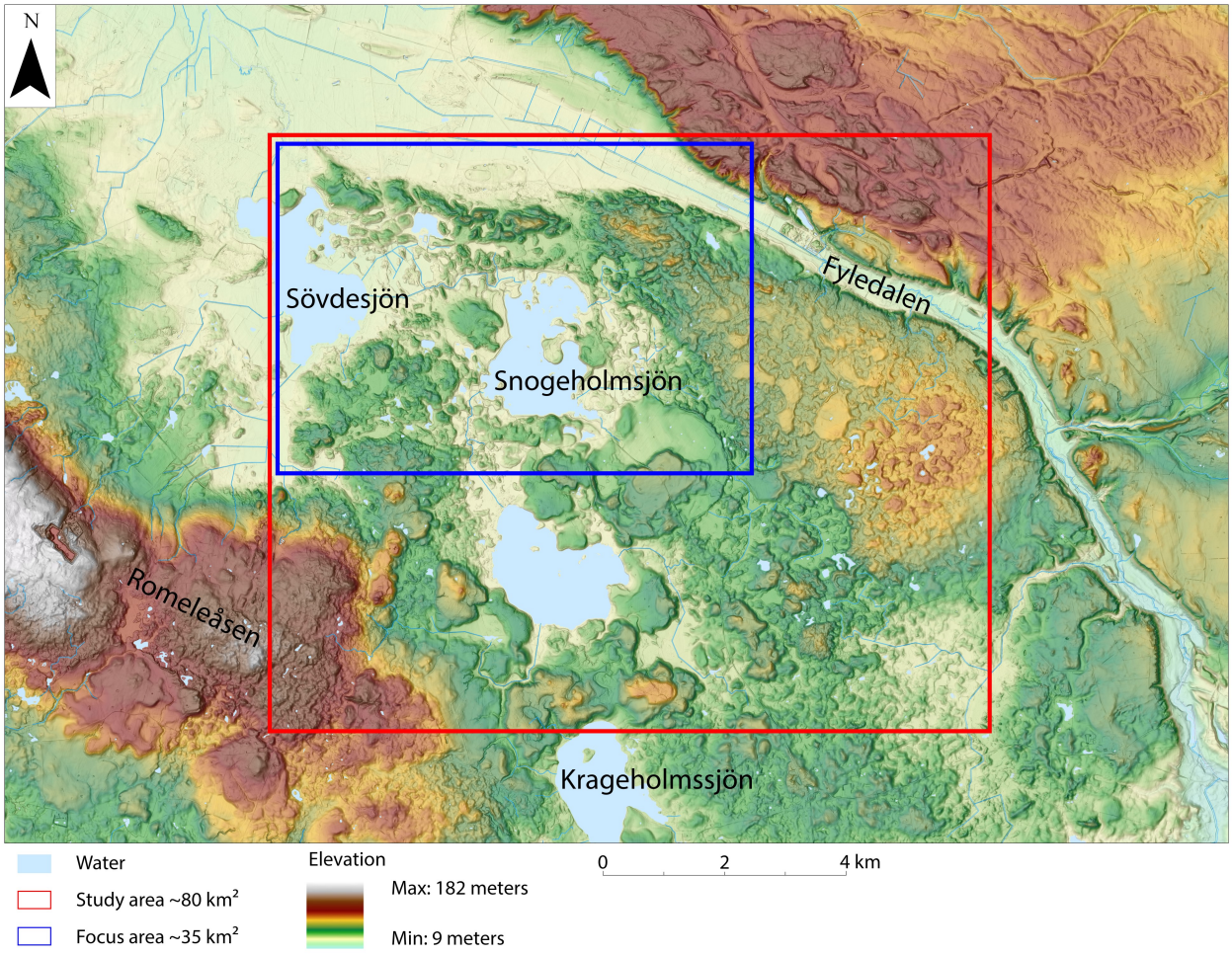

Figure 2. Map showing the extent of the entire study area and of the focus area therein, visible as the red marker on Figure 1. Points of interests that are referenced in text are labeled on the map. The relief is shown with an exaggeration factor of five and a colored elevation profile is applied.

the ice sheet covered the entirety of the Fennoscandian peninsula and reached further southwards covering most of Denmark, northeastern Germany and northern Poland (Fig. 3 map) (Houmark-Nielsen & Kjær 2003; Hughes et al. 2016). The LGM occurred between 22 and 19 ka in different parts of the ice sheet (Stroeven et al. 2016) due to the time-transgressive nature of both advance and retreat dynamics in different parts of the ice sheet, which is a common feature of all ice masses of that size (Hubbard et al. 2009; Benn & Evans 2010; Patton et al. 2017).

After the LGM, the ice started retreating and the ice-margin moved northeastward through the southernmost province of Sweden, Scania. The exact time of the ice-marginal retreat through Scania is quite complex with northwestern Scania starting to become ice-free between 18 and 16 ka as the ice-margin continues to retreat both northwards and eastwards in a time transgressive manner through Scania (Lidmar-Bergström et al. 1991; Houmark-Nielsen & Kjær 2003; Ringberg 2003; Hughes et al. 2016; Stroeven et al. 2016). As a part of the general course of deglaciation, the Lower Baltic Ice Stream was initiated ca 18–16 ka and advanced and moved in through the Baltic Basin while turning westward over Scania and thereafter northwards in the Öresund strait as it fanned out as an ice lobe (Lagerlund 1980; Berglund & Lagerlund 1981; Houmark-Nielsen & Kjær 2003; Houmark-Nielsen 2007, 2010; Anjar et al. 2014; Möller et al. 2019). This change in ice direction, from previously coming in from the north to northeast during the Main Advance, to instead coming in from the east, has been used as an argument in support of dead ice formation in the region, including the study area, based on the reasoning that part of the ice sheet lost its supply of ice (Fig. 4 map) (Lidmar-Bergström et al. 1991). During the movement of the Lower Baltic ice stream over Scania , it is believed that the ice stream moved over large areas covered by dead ice previously disconnected from the FIS (Houmark-Nielsen & Kjær 2003; Kjær et al. 2003), or around partial areas of dead ice (Lidmar-Bergström et al. 1991; Daniel 1992). According to this argument, as the Lower Baltic ice stream diminished, the ice-margin continued to retreat eastwards. As the region south of and including Fyledalen in central Scania became ice-free, a drainage system of interconnected valleys is thought to have developed, merging within Fyledalen. The latter valley system has therefore subsequently been deepened by meltwater erosion, cutting through both glaciofluvial sediments and underlying bedrock (Daniel 1986; Lidmar-Bergström et al. 1991; Daniel 1992). Whilst the general topography of Scania is raised in the northeastern parts, generally causing a drainage toward the southwest, the drainage in Fyledalen appears to have started in the south near the coast and drained north and northwestwards into the Vomb Ice Lake (Fig. 4 map) (Bergsten 1981; Lidmar-Bergström et al. 1991; Daniel 1992) situated at or just above sea level (Hörnsten 1979). The origin of this drainage pattern and the spatial expanse of the Vomb Ice Lake occurred due to the constraints caused by the topography of Romeleåsen (Fig. 2 map), stagnated and dead ice in the south and southwest, and an active ice-margin enveloping the entire valley system in the east (Fig. 4 map). This has been speculated to have caused an ice-dammed lake to form (Lidmar-Bergström et al. 1991; Daniel 1992), creating a drainage route along the northern edge of Romeleåsen (Lidmar-Bergström et al. 1991). The stagnant ice damming up the ice lake gave rise to an uneven landscape predominantly described as hummocky moraine (SGU 1985; Daniel 1986; SGU 1989; Lidmar-Bergström et al. 1991; Daniel 1992), but containing both glaciofluvial deposits and ice-walled lake plains (IWLP) that indicate that glaciofluvial deposition took place both on and around the dead ice (Daniel 1986; Lidmar-Bergström et al. 1991; Daniel 1992). After deglaciation, the region was uplifted due to isostatic rebound, and aeolian sand (often omitted from maps due to thin layers or mapped as glaciofluvial deposits) drapes part of the region, including the hummocks (Daniel 1986, 1992).

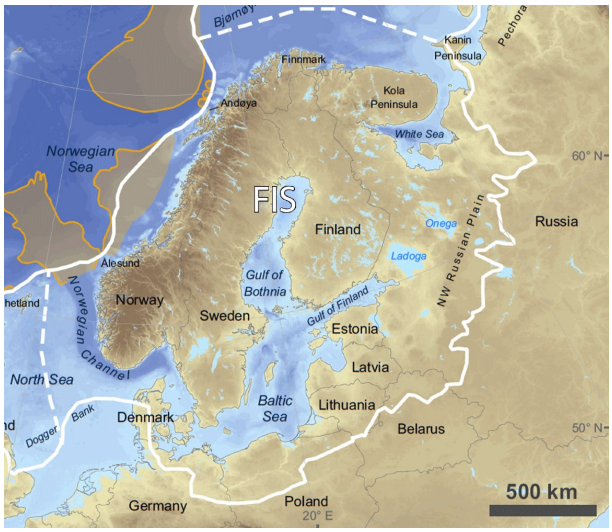

Figure 3. Map focused on the Fennoscandian Peninsula and the extent of the Fennoscandian Ice Sheet during the last glacial maximum. Orange field depict trough mouth fans on the continental shelf. Modified from Hughes et al. (2016).

2.3 Quaternary deposits

During The Quaternary deposits have previously been described by Daniel (1986, 1992) as a supplement to the sediment maps published by SGU (1985, 1989, 2022) (Fig. 5).

The study area is situated above the highest coastline (SGU 2015), with the former glacial lake, Vomb Ice Lake, believed to have been situated at the same level or just above the same level as the as the sea level at that point in time (Lidmar-Bergström et al. 1991).

In the northwestern part of the study area, a vast sandur approximately 30 km long stretches out beyond the study area (Fig. 2 map) (SGU 1989; Daniel 1992), with paleo current measurements indicating paleo current flow directions northwestwards from the mouth of the valley (Fig. 4 map) (Lidmar-Bergström et al. 1991). Some parts around the southern side of current Lake Vomb slope steeply, indicating the location where glaciofluvial sediments was deposited on top of or against a block of dead ice (Lidmar-Bergström et al. 1991).

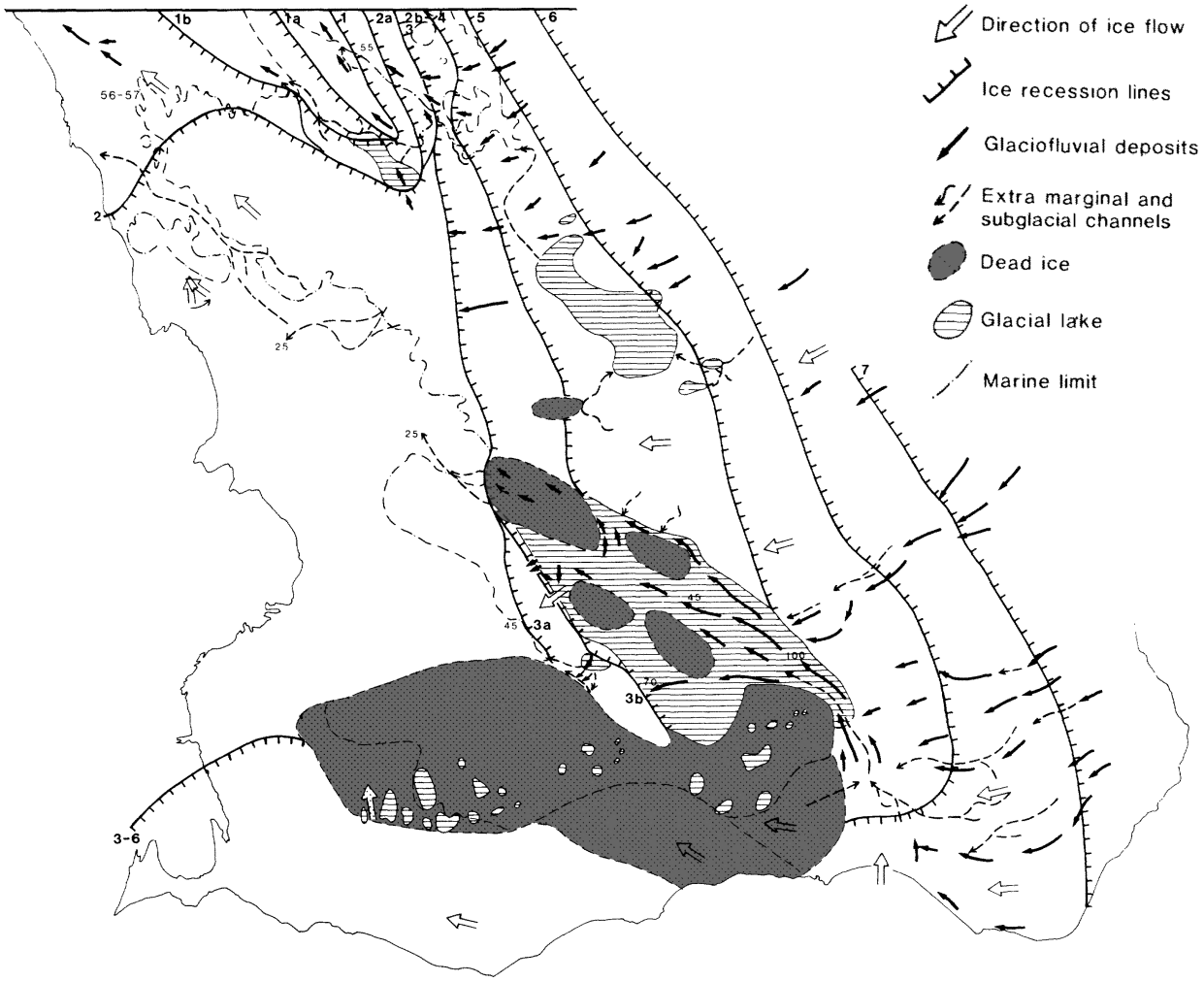

Figure 4. Map showing the different stages of ice-marginal retreat of the Fennoscandian Ice Sheet in Scania, southern Sweden, according to Lidmar-Bergström et al. (1991). Study area marked in red and focus area marked in blue. Seven ice-margins at different stages of retreat are marked at the top of the map that show how the ice-margin retreats eastwards while a stationary ice-margin is present in the south through stages three to six. The map also shows the extent of the reconstructed Vomb Ice Lake and the area in the south thought to have been covered by stagnant or dead ice. Just south of the dead ice the ice sheet is still active with ice-flow toward the west and northwest. Modified from Lidmar-Bergström et al. (1991).

Fyledalen, a fault-guided valley, is situated to the north of the study area, extending further towards the eastern and southeastern sections of the study area (Fig. 2 map). The valley's erosive features incise into the glaciofluvial sediments and in part the sedimentary bedrock, exposing sloped sections 30 to 70 m high down into the valley (SGU 1989; Lidmar-Bergström et al. 1991; Daniel 1992). The valley floor is relatively flat with sections of peat, overbank deposits from river flooding and postglacial (possibly aeolian) sand (SGU 1989).

The area just south of the valley and valley mouth, in the northern part of the focus area, is composed of several long and tall hills that cover an area of roughly 2 by 8 km (Fig. 2 map). These hills are made up of mostly sorted sediments, as observed in several sand and gravel pits around the area (SGU 1989; Daniel 1992), with coarser material toward the top and occasional till interbeds exposed in some locations (Gustafsson 1969; Lindberg Skutsjö 2021). Sediment thicknesses reach up to 50 m (Daniel 1992). The hilly, or hummocky, area was previously believed to have been deposited in, by and around dead ice (Daniel 1992).

Further south of the study area, the landscape has been dominantly labelled as 'hummocky moraine' (Fig. 2 map) (Munthe 1920; Daniel 1986; Lidmar-Bergström et al. 1991; Daniel 1992), with additions of a few other landforms. The area is littered with very small and local deposits of sorted glaciofluvial sediments, most common in the eastern part of the study area (Daniel 1992). The hummocks also contain sorted sediments to some degree, making current and previous classifications of the hummocks inconsistent (Munthe 1920; Daniel 1992). Large parts of the area, and the hummocks, are covered by a thin layer of well-sorted, massive aeolian sand, also contributing to the difficulty of correctly classifying the hummocks according to their genesis (Daniel 1986, 1992). Boreholes from between Lake Sövde and Lake Snogeholm (Fig. 2 map) show a sediment sequence of 75 m with two major till units dominating the sequence with inter-till

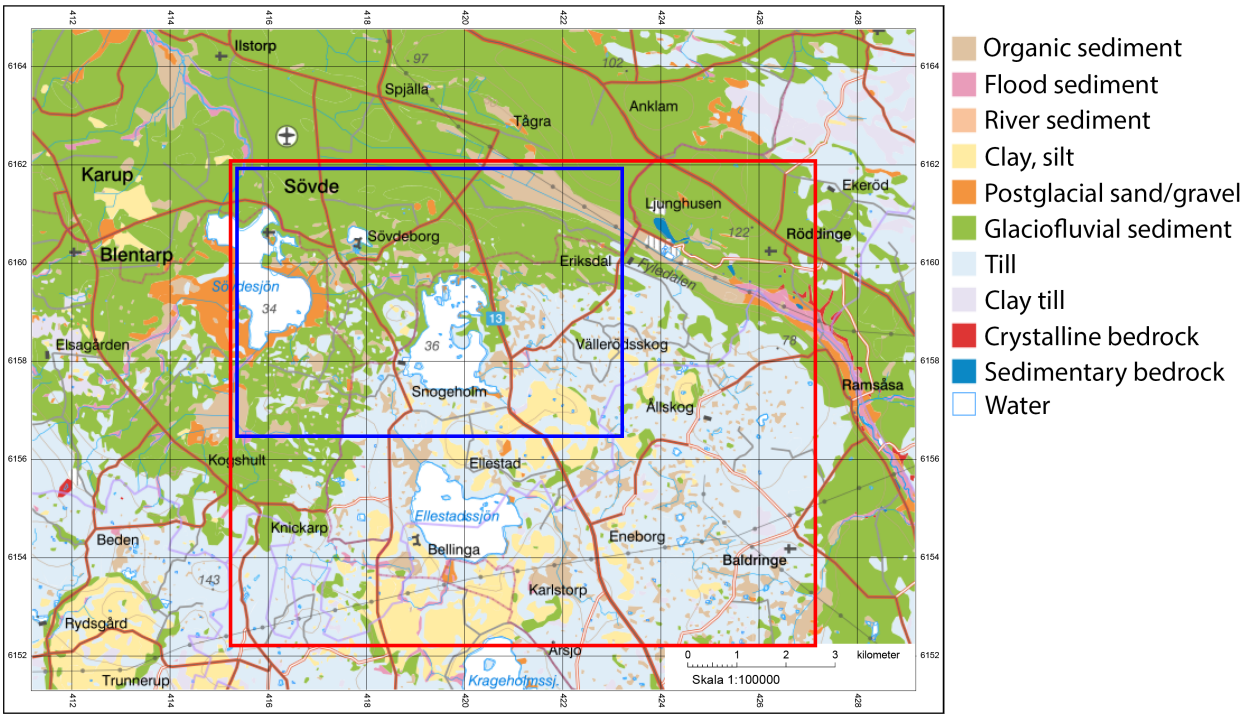

Figure 5. Sediment map over the study area. The digital map is based on the previous maps Ae65 and Ae99 by SGU (1985, 1989). Modified from SGU (2022).

layers consisting of well-sorted clay, silt and sand (Nilsson 2013; Lindberg Skutsjö 2021). The lower areas between the hummocks are covered with "glacial" sand up to a thickness of 5 m (Daniel 1992). In between the hummocks, flat areas consisting of peat have been interpreted to have formed in dead ice depressions (SGU 1989; Daniel 1992).

In addition to the landscape dominated by hummocky moraine the study area contains several clay plateaus (SGU 1989; Daniel 1992). These have been interpreted as IWLPs (Westergard 1906; Sundberg 2000). These plateau-like features are generally more frequent in the central to eastern parts of the study area (Fig. 2 map). Most often they are circular to semi-circular in shape, with a flat top, and vary in size from around 100 m up to around 2.5 km in diameter (SGU 1989). The plateaus are often made up of glacial clay in the middle and are often surrounded by a raised edge of glaciofluvial sediments with steep slopes outwards that show signs collapse as the supporting ice has melted away. In several cases, the original extent and shape is difficult to discern due to severe post-depositional erosion, including by agricultural and infrastructural practices. The smaller plateaus often lack both the clay and other glaciofluvial sorted sediments, containing only diamictic sediments, interpreted as till (Daniel 1992).

3 Methods

3.1 Remote sensing data analysis

In order to achieve the aims of this thesis, the following methods were employed: geomorphological mapping of the study area was conducted at two different levels of detail (Fig. 2) and split into remotely-sensed and field mapping stages. The geomorphological mapping was conducted in a way that allowed both qualitative and quantitative analysis to be performed later. The geomorphological mapping was followed by a selection of study sites where field work was conducted. Exposures were excavated, logged and sedimentologically analysed.

3.1.1 Datasets and derived functions

Remote sensing data analysis was conducted using several datasets in the software ArcGIS Pro version 2.5.2 by ESRI. A dataset containing LiDAR measurements provided by Lantmäteriet named *GSD-Höjddata grid 2+* (Table 1) (Lantmäteriet 2020) and compiled

Table 1. List of the datasets used in the remote mapping of the study area. The datasets are compiled by the government agencies Lantmäteriet and Sveriges Geologiska Undersökning (SGU) and supplied by the Geodata Extraction Tool provided by the Swedish University of Agricultural Sciences (SLU).

Dataset name	Content description	Resolution/scale/accuracy	Source	Date
GSD-Höjddata grid 2+	LiDAR data compiled into a DEM	2 m horizontal, 0.1 m vertical	Lantmäteriet	2020
GSD-Fastighetskartan vektor	Hydrology	Linear objects minimum 6m wide and 200m long; Surface areas larger than 400 sqm.	Lantmäteriet	2019
Ortofoto	Orthophotos	0.16 to 0.5 m per pixel	Lantmäteriet	2019
HÖGSTA KUSTLINJEN	Highest coastline	50 m horizontal, 2 m vertical	SGU	2015
JORDARTER 1:25 000-1:100 0000	Soil and sediments	1:25 000 to 1:100 00	SGU	2014
BERGGRUND 1:50 000-1:250 000	Bedrock and basement information	1:50 000 to 1:250 000	SGU	2017

into a DEM was used as the main dataset for the remote mapping of landforms and associated analysis. The LiDAR data is of the vertical resolution of 0.1 ±0.05 m and horizontal resolution of 2 ±0.25 m with the average point density of measurements in the dataset being 0.5–1 points per m2 (Lantmäteriet 2019). This resolution is more than adequate for the mapping of glacial landforms (Dowling et al. 2013). The dataset is pre-processed to remove the cover of vegetation to only present the topography underneath, as well as to flatten water surfaces. The DEM was processed into several different raster models for visual processing and qualitative interpretation to map landforms, as polygons in the study area. This was later used for both quantitative and qualitative analysis.

A multidirectional hillshade model and raster layer was created by calculating and merging multiple directional sources of light from a multitude of azimuths and angles while projecting these onto the DEM, creating shadows exposing the relief of the landscape (Fig. 6). Using a multidirectional hillshade model instead of the more traditional directional hillshade model helped avoid landform bias towards a single azimuth (Smith & Clark 2005; Hughes et al. 2010), while also ensuring adequate illumination and coverage of the landforms (Margold & Jansson 2012). The hillshade model is presented in grayscale to display the contrasts between shadows and corresponding light sources and utilizes a 5x vertical exaggeration (Fig. 6).

Three slope raster layers were created by comparing adjacent points of elevation within the DEM to calculate slope steepness over the entire region in the same vertical and horizontal resolution as the original DEM (Fig. 7). The three slope raster layers each had

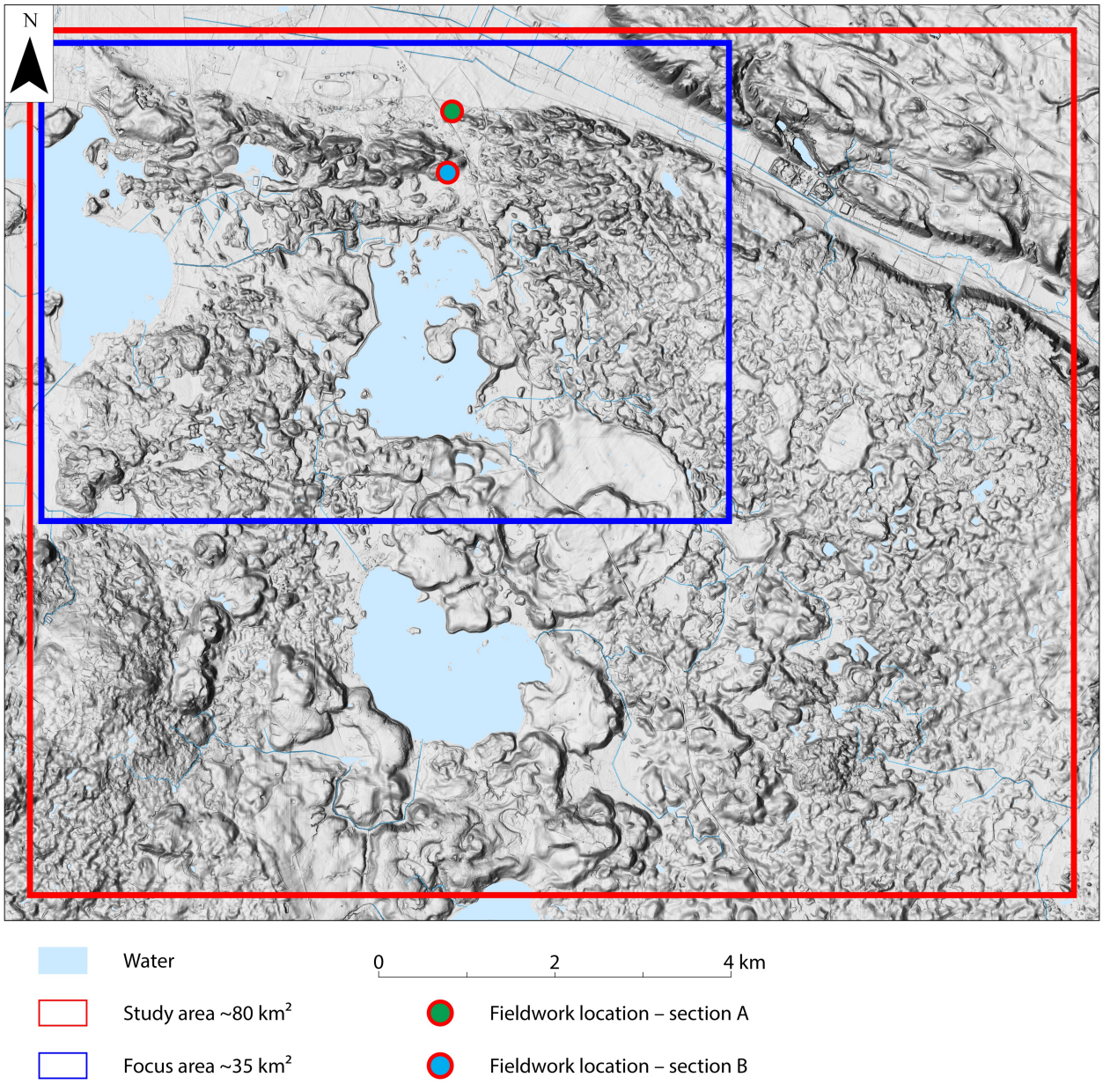

Figure 6. Hillshade model of the study area based on the DEM by Lantmäteriet (2020). Light sources are multidirectional to avoid azimuth bias and the vertical relief is exaggerated by a factor of five.

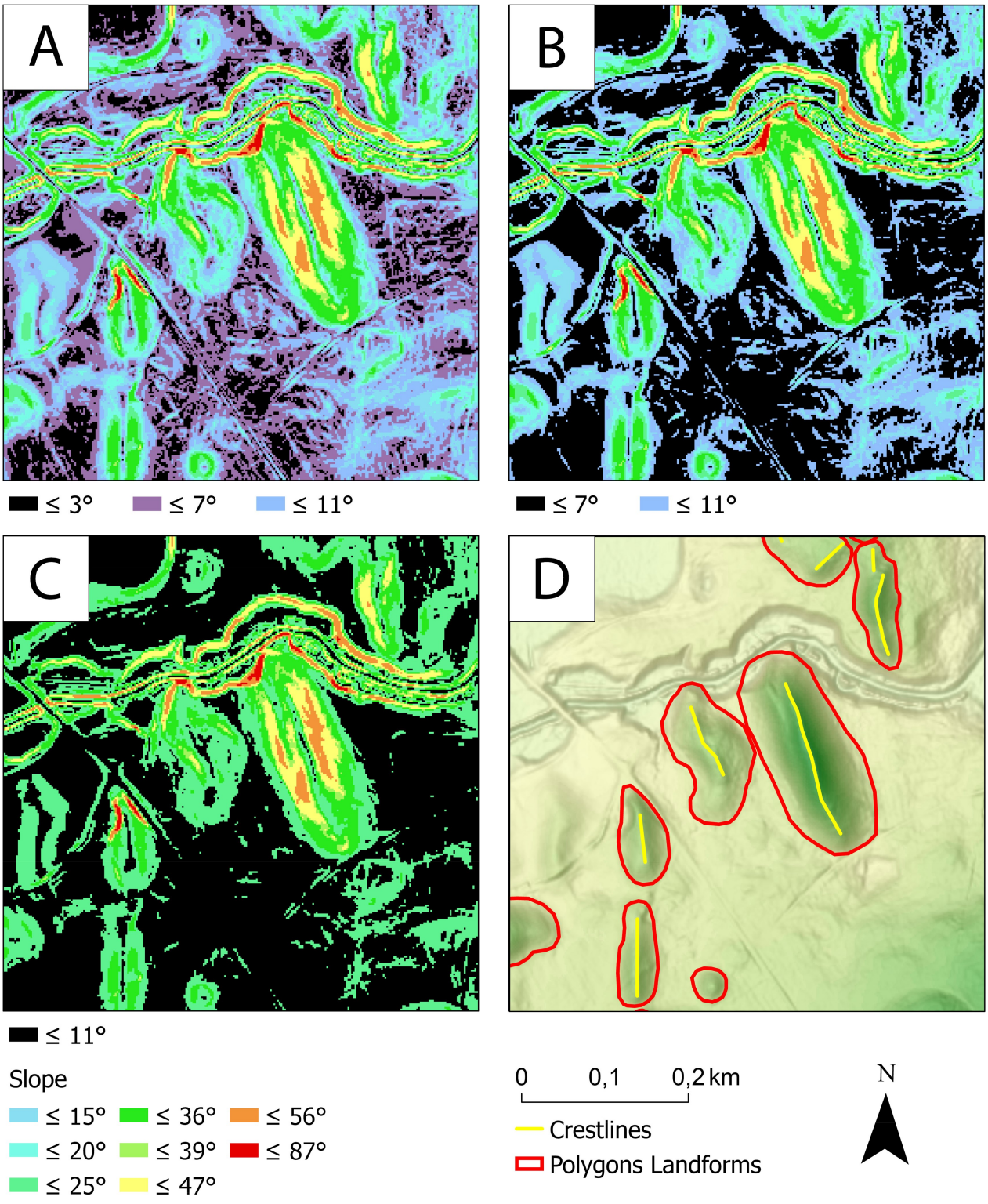

Figure 7. Three figures (6a, 6b, 6c) showing different slope symbology to indicate slope steepness, providing a basis for interpreting the breaks of slope with varying degree of background noise. Figure 6d has no slope raster applied but an elevation profile instead, with darker colors indicating a higher elevation to differentiate between lower and higher breaks of slope. Figure 6d contains the results with the red polygon marking the landform according to the interpreted lower break of slope and the yellow lines marking the interpreted crestlines.

the upper limits of slope angles defined as 3°, 7° or 11° to distinguish a sloped surface from a horizontal or near-horizontal one. Thus, the different raster layers indicate that a surface is horizontal when the slope value is less (more flat) than either 3°, 7° or 11° incline, depending on the raster layer (Fig. 7). This was to be used as a tool when interpreting the break of slope, as they provide different levels of background noise to the raster layer (Fig. 7). This made no differentiation between lower and higher breaks of slope, meaning that both the bottom and top of a hill are both displayed as horizontal.

A colour ramp to indicate elevation above sea level was created based on the elevation data within the DEM in the form of a transparent masking layer (Fig. 2). This layer helps to distinguish between lower and higher breaks of slope and could be applied to any other raster layer. The colour ramp has the same vertical and horizontal resolution as the DEM.

In addition to the DEM and the raster layers derived from it (hillshade model, slope rasters and elevation profile), several additional datasets were used simultaneously to verify and cross-reference the results from the remote sensing. These include hydrology; soil and sediments; bedrock; orthophotos; and the highest coastline. The datasets are presented in full in *Table 1*.

3.1.2 Approach to geomorphological mapping

The approach taken when classifying glacial landforms during mapping is mostly based on that of Hughes et al. (2010) and Chandler et al. (2018) using visual identification through the use of a multidirectional hillshade model, break of slope and elevation in relation to surroundings; with the addition of IWLPs according to the morphological descriptions of circular shapes with flat tops and a raised rim, together with sediment facies association of clay, glaciofluvial sediment, and till, described by Clayton et al. (2008).

Mapping landforms through remote sensing data was performed in the software ArcGIS Pro version 2.5.2 by ESRI through qualitative visual identification of each individual landform and outlining it with a polygon. The majority of the work was performed using the multidirectional hillshade model, slope rasters and coloured elevation profile that were derived from the DEM supplied by Lantmäteriet (2020). The aim of these layers is to distinguish the lower break of slope and to trace it to outline the landform as a polygon. The polygon is then cross-referenced with orthophotos and hydrology data to exclude anthropogenic influences on the overall shape of the landform. In case several landforms being indistinguishable or partially indistinguishable from each other, a composite landform was traced or distinctive sub-features were mapped instead. Further properties such as minor or major anthropogenic impact, cross-cutting relationships, overprinting, lobate shapes and crestline bifurcations were noted and the information tied to specific polygons. In addition to the previous mapping of landforms through the lower breaks of slope, crestlines were also mapped and traced as polylines and tied to a previously mapped polygon. After the mapping of landforms, crestlines, and properties, the results were reviewed twice to ensure consistent results across the entire study area.

3.2 Field work

3.2.1 Selection of study sites

A preliminary selection of 15 suitable locations within the 80 km2 study area was based on the geomorphological mapping. Due to the general size of the landforms which are often at a scale of hundreds of meters, old sand- and gravel pits were deemed desirable locations for excavation. Of these 15 locations, four were selected for further excavation after field visits, with a total of five sections being dug out in an alignment as close to perpendicular to the crestline as possible. Two of these five sections proved to be amenable to creating sections of sufficient dimensions to warrant further sedimentological analysis and logging. Section A is located at N55.5889°, E13.7339° and section B is located at N55.5836°, E13.7314° referenced to the geodetic system SWEREF 99 TM. All other sections had either collapsed, planed off after pit abandonment or had too many tree roots that hampered meaningful progress.

3.2.2 Sedimentology

The exposures were excavated by hand using shovels and trenching tools, and subsequently cleaned up with a trowel. The exposures were systematically photographed and logged as sections according to the methodology of Evans & Benn (2021) with unit- and structural-geological measurements taken in the field. Photos of the sections were merged into a mosaic to provide as much detail as possible while simultaneously keeping the distortion to a minimum. Lastly the logs were digitized to match the photos and mosaic in the software Adobe Photoshop 2017. The logs contain information about lithofacies, unit boundaries, faults and deformation structures, laminations and clasts; terminology follows the scheme of Benn & Evans (2010) and Evans and Benn (2021).

Structural measurements were taken by creating a three-dimensional cut out in the exposure and inserting a plastic board tracing the layer or structure in question, hence projecting a plane outwards that could be measured using a compass-clinometer (Evans & Benn 2021). The structural measurements taken were dip and dip azimuth, subsequently plotted as plane features using the software Stereonet version 11 (Allmendinger et al. 2012; Cardozo & Allmendinger 2013).

4 Results

4.1 Remote sensing data analysis

During the geomorphological mapping and subsequent review of the remote sensing data a total of 367 landforms were mapped as hummocks and represented as polygons. These hummocks possessed a total of 691 crestlines that were mapped as polylines. An additional 41 landforms were mapped as larger, flat-topped circular features without crestlines and thus interpreted as IWLP and represented as polygons.

Large parts of the study area have been subjec-

ted to a substantial amount of farming and agriculture. This results in a heavy decline of the relief and individuality of subjected landforms causing the quality and certainty of the geomorphological mapping to substantially drop in specific areas (Fig. 8). This leads to a stark contrast in mapping detail: while an almost complete map of the focus area could be created, only major distinguishable features were mapped outside of it.

4.1.1 Ice-walled lake plains

The results of the geomorphological mapping of the remote sensing data at an overview scale of the study area are presented in *Figure 8*. The IWLPs are best viewed at this scale and can be seen as major features of the landscape. A total of 41 IWLPs were identified according to the criteria of Clayton et al. (2008). It was only in a few cases that all criteria were applicable. The overall factors taken into consideration and together formed a qualitative grade of certainty for landform classification are presented in *Table 2* and include the overall shape, potential erosion, sediments present according to previous mapping of SGU (1985, 1989, 2014), raised elevation compared to surrounding hummocks, and the presence or absence of a raised rim.

It can be seen that there is a larger concentration of IWLPs in the eastern part of the study area than in the western part (Fig. 9). The sizes vary greatly, with the smallest IWLP measured at as little as 260 m across with a 15338 m2 surface area, and the largest IWLP measuring 2.6 km across and a 4.19 km2 surface area, which amounts to a 273-fold size difference.

4.1.2 Hummocky terrain

The Hummocky terrain is present and mapped in the northwestern part of the study area (Fig. 9). A total of 367 hummocks represented as polygons were mapped and enclosed in a rectangle representing the bounding geometry with the smallest width possible. The elongation ratio was calculated using this bounding rectangle and 283 hummocks show an elongation ratio of 1.5 or more. The hummocks were further divided according to the size of the surface area represented by the mapped polygons, with smaller hummocks defined as ≤ 40 000 m2 and larger hummocks as ≥ 40 000 m2 (Fig. 10). The focus area was divided into four smaller parts and the orientation of the bounding rectangles were plotted as stereonets with an equal area polar grid projection. The orientations of the bounding rectangles are treated as axes without dip and therefore presented as both normal and mirrored data in the stereonets (Fig. 10), meaning an azimuth of 91° adds two data points as both 91° and 271° to represent an axis running through a central focal point. Lastly, the elongated hummock orientations of all four areas were compiled and summarised in several stereonets (Fig. 11).

In the northwestern part of the focus area 21 large hummocks were mapped with a mean orientation of 104 ±14° and eigenvalue S1=0.7944, and 40 smaller hummocks with a mean orientation of 146 ±17° and an S1=0.6795 (Fig. 10). In the northeastern part of the

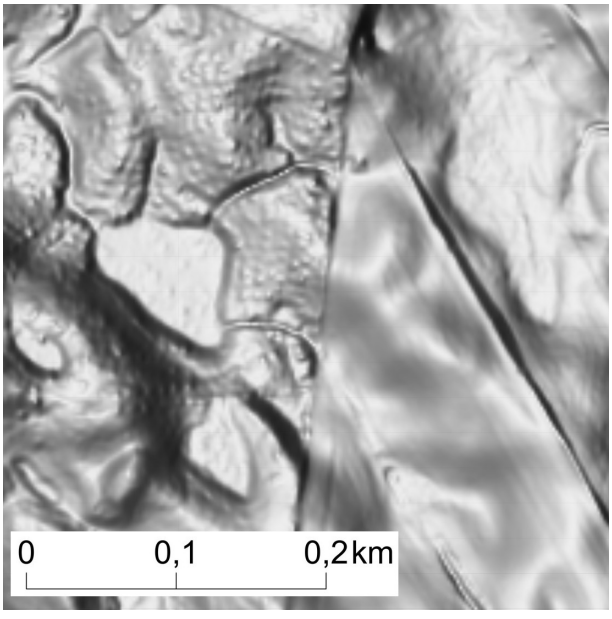

Figure 8. Hillshade model showing how substantial agriculture smoothes and blurs the relief in the right of the figure. The border between unfarmed land to the left and farmed land to the right has arisen due to different land use.

Table 2. Table presenting a summary of the criteria when mapping ice-walled lake plains in the study area. Of the 41 mapped ice-walled lake plains 17 were deemed certain, 13 were deemed likely, and 11 were deemed to have been classified with some degree of uncertainty.

ID	Sediments according to previous mapping by SGU inside the polygon			Surface area (sqm)	Classification certainty
1	Glacial clay	Glacifluvial sediment	Till	4194739	Certain
2	Glacial clay		Till	420377	Certain
3	Glacial clay		Till	560974	Certain
4	Glacial clay		Till	212516	Certain
5	Glacial clay	Glacifluvial sediment		299935	Certain
6		Glacifluvial sediment	Till	52494	Certain
7	Glacial clay	Glacifluvial sediment		454857	Certain
8	Glacial clay	Glacifluvial sediment	Till	383057	Certain
9			Till	95524	Certain
10		Glacifluvial sediment	Till	98112	Certain
11	Glacial clay	Glacifluvial sediment	Till	164624	Certain
12		Glacifluvial sediment	Till	67742	Certain
13		Glacifluvial sediment	Till	298171	Certain
14	Glacial clay	Glacifluvial sediment	Till	947264	Certain
15	Glacial clay		Till	789283	Certain
16	Glacial clay		Till	440367	Certain
17	Glacial clay		Till	241151	Certain
18	Glacial clay		Till	45413	Likely
19	Glacial clay		Till	60329	Likely
20		Glacifluvial sediment	Till	53657	Likely
21		Glacifluvial sediment	Till	243985	Likely
22	Glacial clay	Glacifluvial sediment	Till	530430	Likely
23		Glacifluvial sediment	Till	100456	Likely
24			Till	85025	Likely
25			Till	92037	Likely
26			Till	89090	Likely
27	Glacial clay		Till	138128	Likely
28	Glacial clay	Glacifluvial sediment	Till	1005554	Likely
29	Glacial clay		Till	28707	Likely
30			Till	113495	Likely
31		Glacifluvial sediment	Till	195439	Uncertain
32			Till	60141	Uncertain
33			Till	15338	Uncertain
34			Till	55926	Uncertain
35			Till	54120	Uncertain
36			Till	75702	Uncertain
37	Glacial clay		Till	306364	Uncertain
38	Glacial clay		Till	239299	Uncertain
39	Glacial clay		Till	222145	Uncertain
40			Till	165065	Uncertain
41	Glacial clay	Glacifluvial sediment	Till	311668	Uncertain

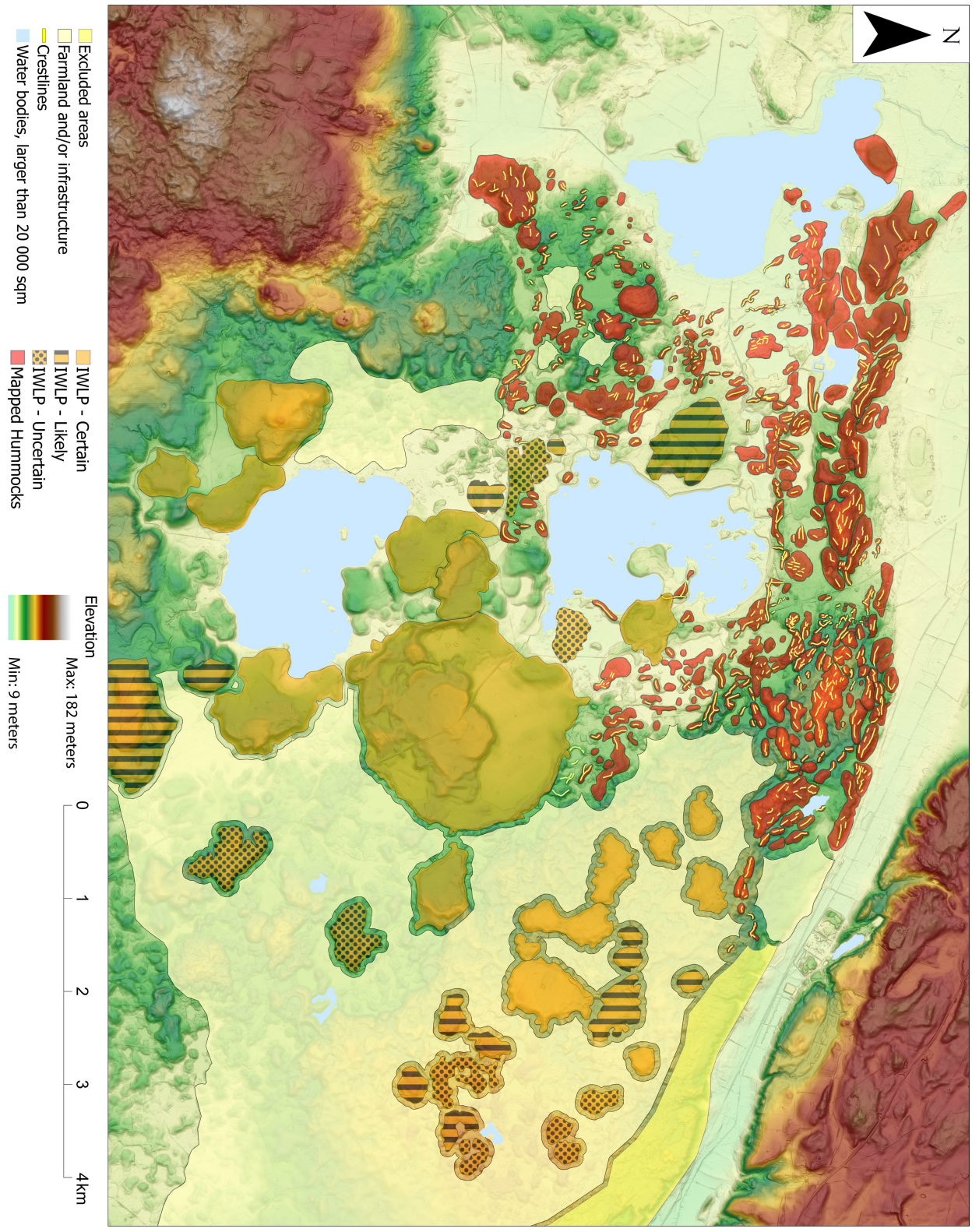

Figure 9. Map showing the results of the complete geomorphological mapping at an overview scale. The base is a hillshade model based on the DEM by Lantmäteriet (2020) and the vertical relief is exaggerated by a factor of five and a colored elevation profile is applied.

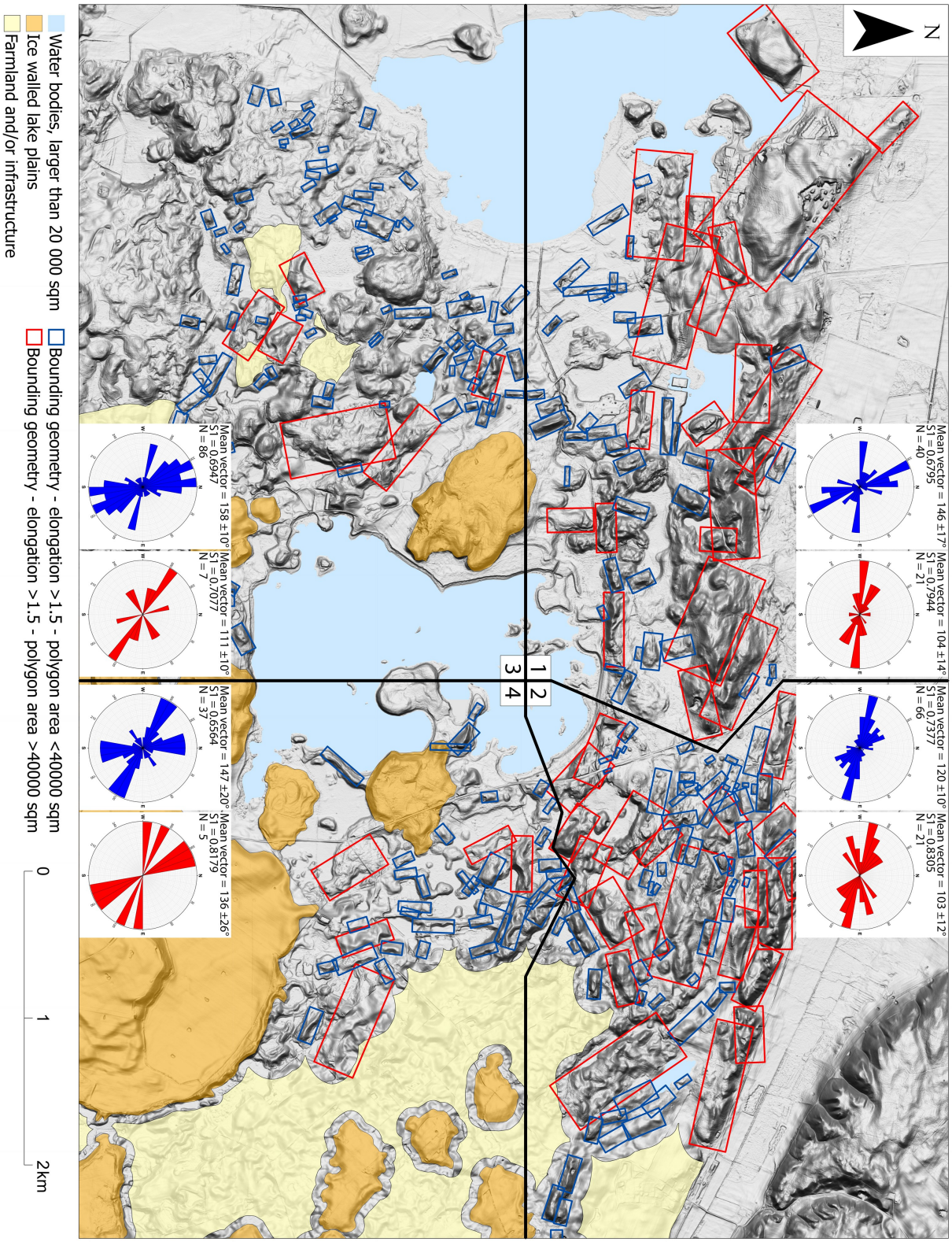

Figure 10. Map showing the previously mapped landforms seen in Figure 8 with an elongation ratio of ≥ 1.5, and the polygon geometry bounded inside rectangles with the smallest possible width. The map is divided into four parts with associated stereonets showing the strike of the bounding geometry in a mirrored format. Blue stereonets correspond with landforms smaller than 40000 m2, and red stereonets with landforms larger than 40000 m2.

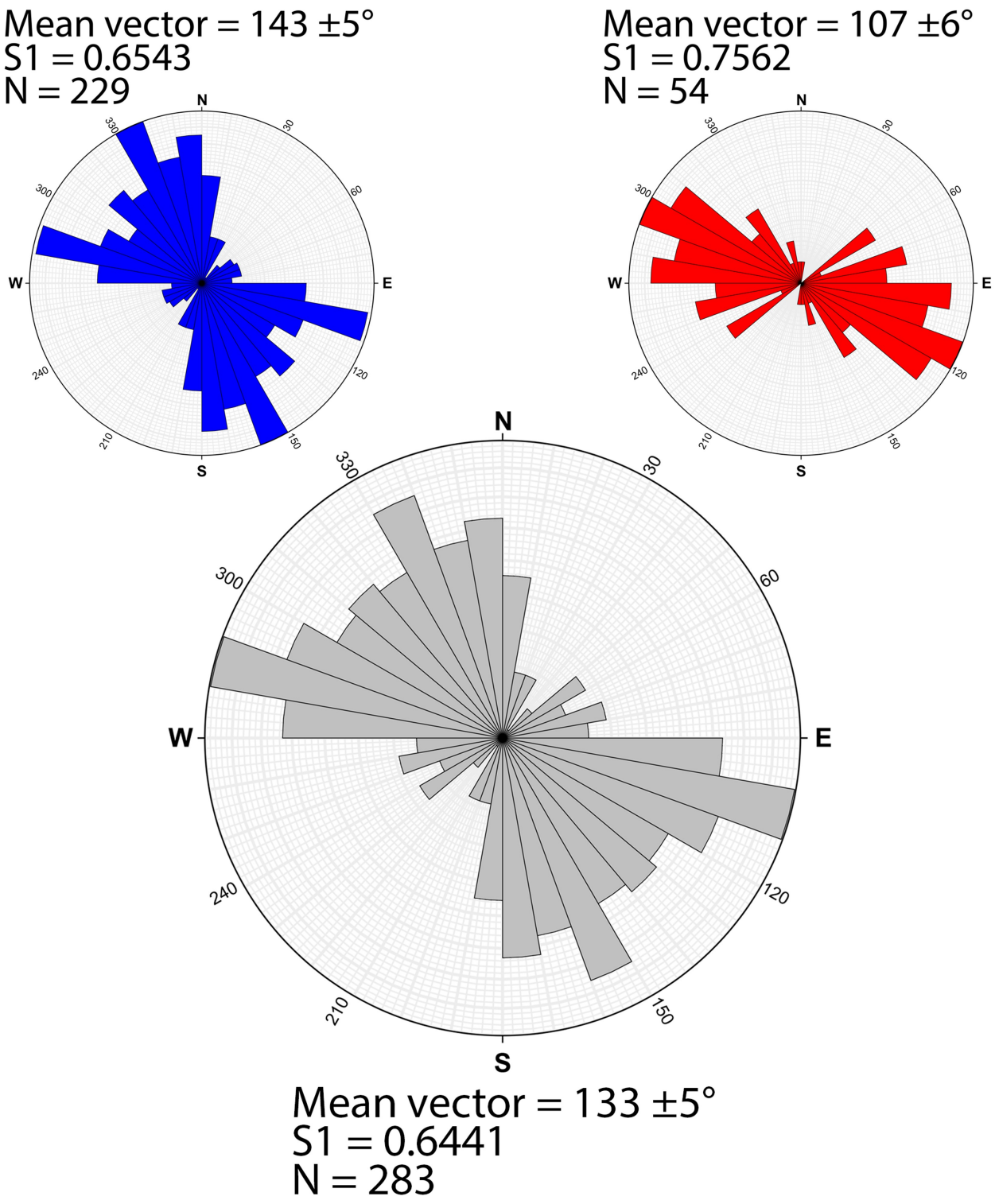

Figure 11. Three stereonets showing the combination of stereonets for the elongated landforms as depicted in Figure 9. Blue stereonets correspond with landforms smaller than 40000 m2 and red stereonets with landforms larger than 40000 m2. The grey stereonet is a combination of both large and small elongated landforms.

focus area 21 large hummocks were mapped with a mean orientation of 103 ±12° and S1=0.8305 and 66 smaller hummocks with a mean orientation of 120 ±10° and an S1=0.7377 (Fig. 10). The fairly high eigenvalues indicate a medium to strong trend in clustering, in this case of hummock orientation (Woodcock 1977; Evans & Benn 2021). The orientation of the large hummocks in the northwest match well with both the large and small hummocks in the north east, with an approximate orientation of WNW to ESE (Fig. 10). The small hummocks in the northwest with its lower eigenvalue (S1) are orientated more along NW to SE.

In the southeastern part of the focus area seven large hummocks were mapped with a mean orientation of 111 ±10° and eigenvalue S1=0.7077; and 86 smaller hummocks with a mean orientation of 158 ±10°, with eigenvalues S1=0.6947 (Fig. 10). In the southeastern part of the focus area five large hummocks were mapped with a mean orientation of 136 ±26° and eigenvalue S1=0.8179; and 37 smaller hummocks with a mean orientation of 147 ±20°, with eigenvalues S1=0.6564 (Fig. 10). The eigenvalues are generally slightly lower in the southern part of the focus area compared to the northern part, but still indicate a medium to strong trend in hummock orientation (Woodcock 1977; Evans & Benn 2021).

The hummocks in the south exhibit a slightly more scattered orientation compared to the north in regards to the larger hummocks, which could be explained by the small sample pool of N=7 for the southwest and N=5 for the southeast. The smaller hummocks in the southwest match well with the smaller hummocks in the southeast, with an approximate orientation of NNW to SSE (Fig. 10). It is noted that there are small differences between the larger and smaller hummocks with the overall orientation for all 283 elongated hummocks at 133 ±5° and eigenvalue S1=0.6441 (Fig. 11).

4.2 Sedimentology

Two sites with one section each were selected for sedimentological analysis and logging, and named section A and section B. The study sites are located in the focus area, and both the study sites and sections are described in detail under chapters 4.2.1 and 4.2.2.

4.2.1 Section A – description

Section A is located in an old, abandoned sandpit on the northern side of a 580 m long and 150 m wide hummock in the northern part of the study area (N55.5889°, E13.7334°; Fig. 6). The hummock displays a western to eastern orientation (280° to 100°). An exposure 2 m wide and 2.5 m high was cleared at broadly right angles to the crestline on the eastern side of the sandpit. The exposure is located approximately halfway up from the base of the hummock. A mosaic was constructed (Fig. 12) using 12 detailed photos of the exposure and used as the base for a digitised 2d-log (Fig. 13). The exposure was divided into five major units, labelled A–E, starting from the bottom.

All five units consist of well-sorted fine to medium sand light in colour, with different amounts of dark bedding planes or laminae of the same grain size as the lighter sand running horizontally.

Unit A. This unit makes up the lowermost 75 cm of the section with the lower contact disappearing beneath the exposure (Fig. 12; Fig. 13). The sediment is made up of a light coloured fine to medium sand, with thin lines of darker sand, likely manganese, as horizontal bedding planes or lamination (Sh). Toward the bottom of the unit there is a higher concentration of darker lamination compared to the middle and top of the unit (Fig. 12). The unit is also dissected by seven reverse faults evenly spaced 10–15 cm apart with apparent displacement ranging from 1–15 cm. Two reverse fault planes were measured averaging a dip direction of 040 ±26° NE and dipping 32 ±4° (Fig. 13).

Unit B. The unit is about 60 cm thick containing fine to medium sand (Sh) but thinning out to the right, with a sheared but clear contact displaying interfingering with Unit A (Fig. 12; Fig. 13). The contact between Unit A and B is sharp and dips 10° toward 026° NNE. The unit displays a high concentration of darker horizontal lamination throughout. The evenly-spaced reverse faults of unit A continue upwards into and through unit B unhindered but bifurcate several times towards the top of the unit. One fault plane was measured as a dip direction 350° N with a 30° dip. Toward the top of the unit the horizontal lamination curves upward towards the upper contact due to shearing at a scale of up to 10 cm.

Unit C. This unit of sand in the form of a wedge has a varying thickness of 2–15 cm (Fig. 12; Fig. 13). It is dissected by several hydrofractures at an apparent right angle compared to the hydrofractures of unit B. The sand is massive without any of the obvious laminations of the other units (Sm). No offset along the fractures can be observed, either as a lack of actual displacement or the lack of lamination and marker layers to reveal this characteristic. The contact toward the underlying unit B is sharp and fairly even, but the contact plane could unfortunately not be measured.

Unit D. The unit is made up of a light-colored fine to medium sand, reaches a maximum thickness of 40 cm and thins out to the west (Fig. 12; Fig. 13). The unit displays the same kind of horizontal lamination and reverse faults as unit A, albeit with smaller amounts of displacement ranging from 1–5 cm (Sh). In addition, a few reverse faults run at an apparent right angle to aforementioned faults in an anastomosing pattern. The contact between the underlying unit C and unit D is sharp and dips 24° toward 190° S. Toward the bottom of the unit the lamination curves slightly downwards toward the contact at a scale of 1–2 cm due to shearing. Two fault planes were measured intersecting at a right angle and orientated almost opposite each other (Fig. 13; Fig. 14).

Unit E. Unit E is divided into three subunits due to the nature of the exposure and these are laterally and vertically connected to each other (Fig. 12; Fig. 13). The total thickness of unit E is estimated at ~150 cm with the upper contact disappearing above the exposure.

Subunit E1. This unit consists of fine to medium sand (Sh) and is 40 cm thick while thinning out towards the east, with the upper contact disappearing above the cleared exposure (Fig. 12; Fig. 13). The unit

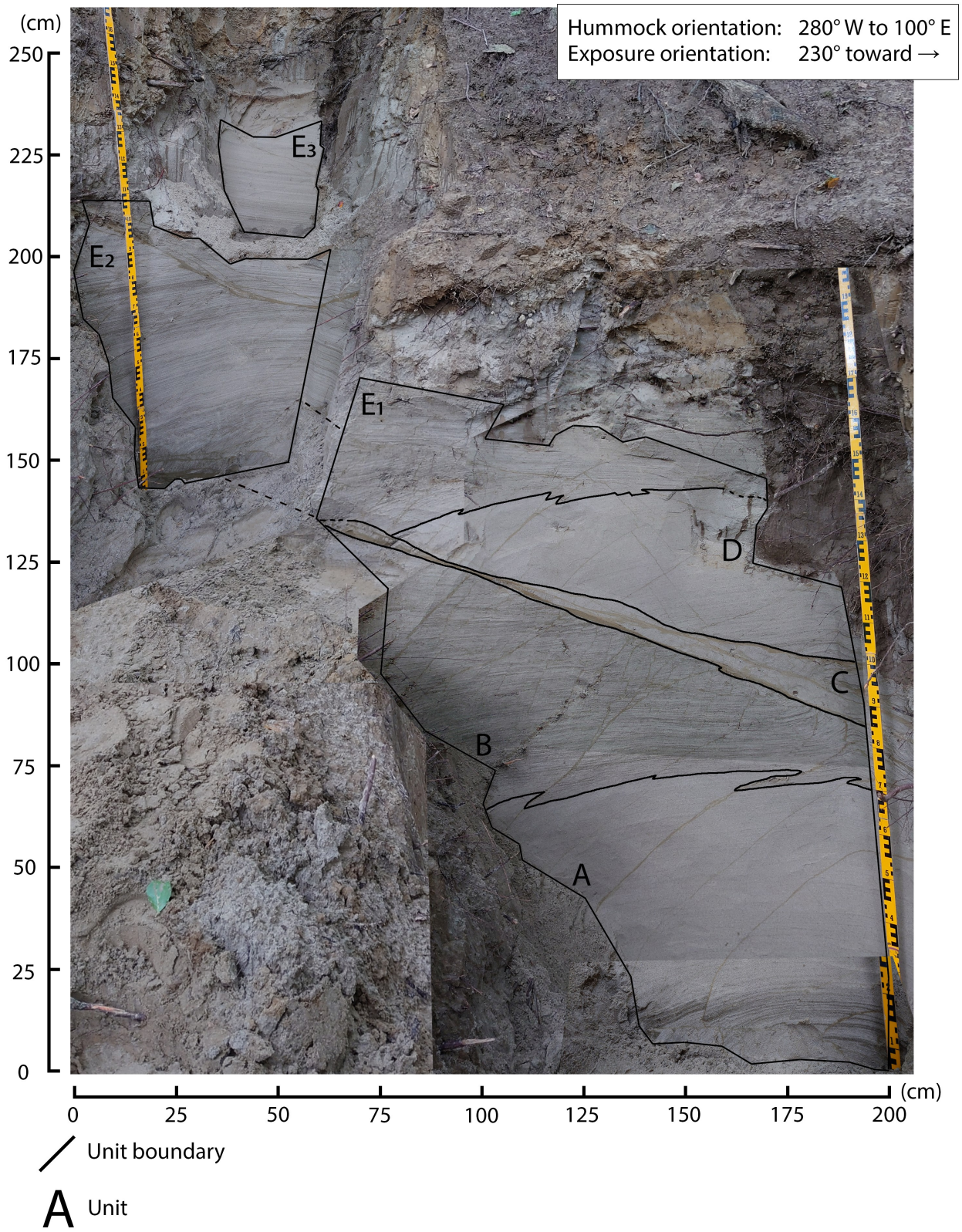

Figure 12. Mosaic constructed from 12 detailed photos showing the exposure of section A. The exposure is 2 m wide and 2.5 m tall and is divided into five major units, from which unit E was divided into three sub units. The sediments are all fine to medium sand with fine lamination, and several reverse faults permeates the entire section.

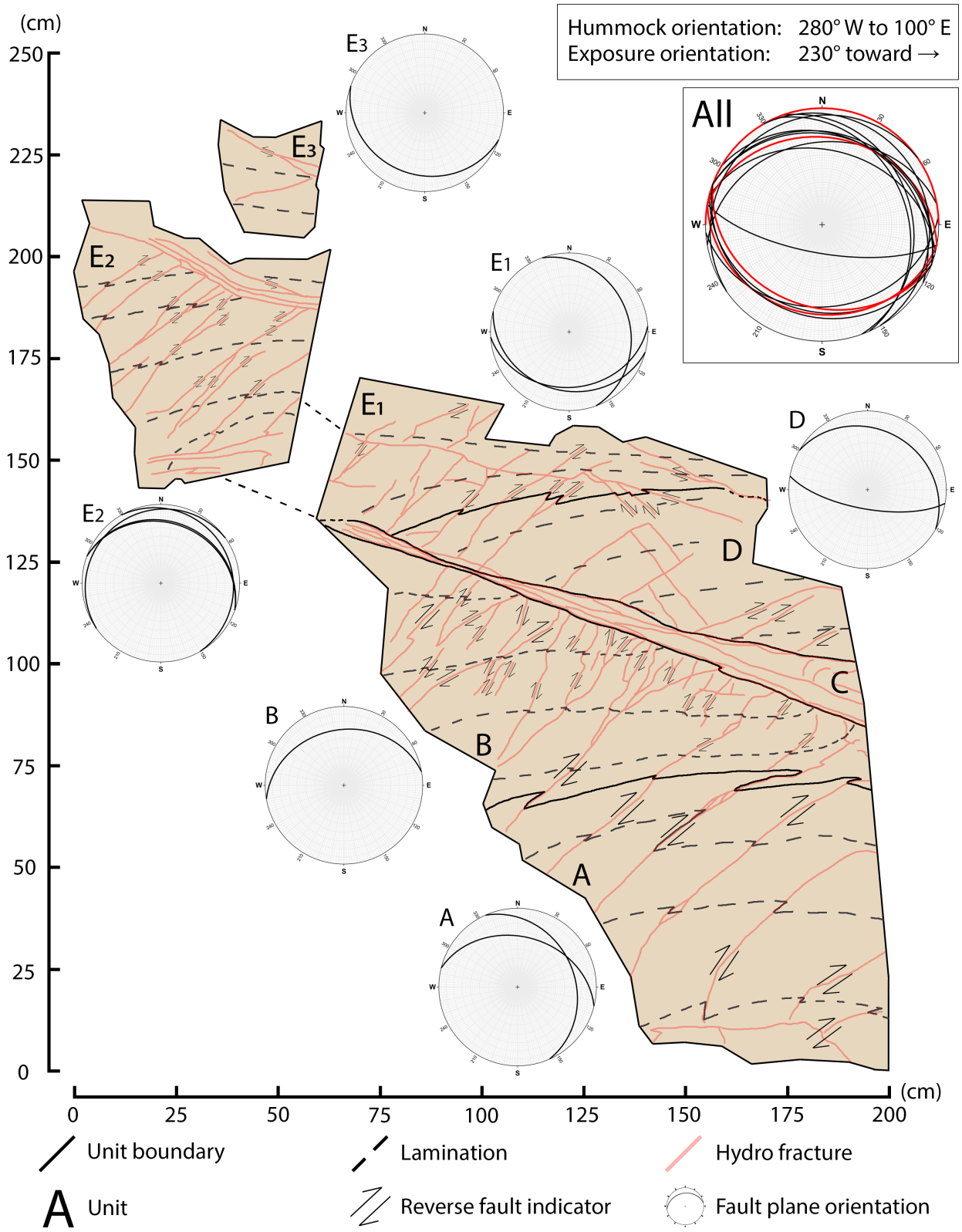

Figure 13. 2d-log of the exposure in section A, as also seen in Figure 10. Stereonets A to E3 show measured fault planes corresponding to the units with the same label. The combined results of all stereonets are found in the top right corner, with the addition of the measured contacts between the units marked as red projections.

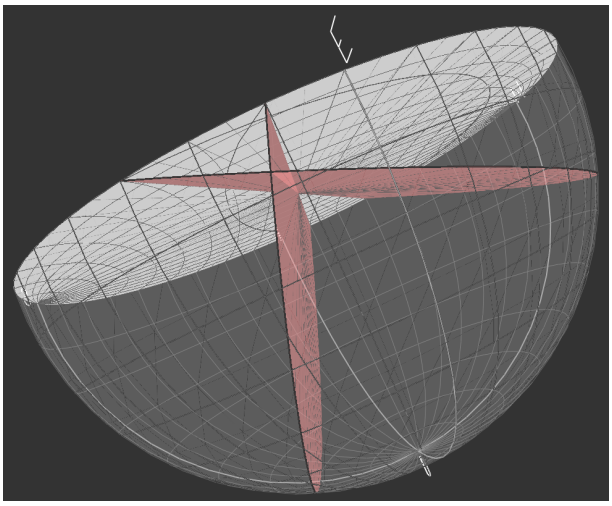

Figure 14. Depiction of the two measured fault planes of unit D in section A as they intersect. The intersecting angle is 86°, at 170° opposite each other.

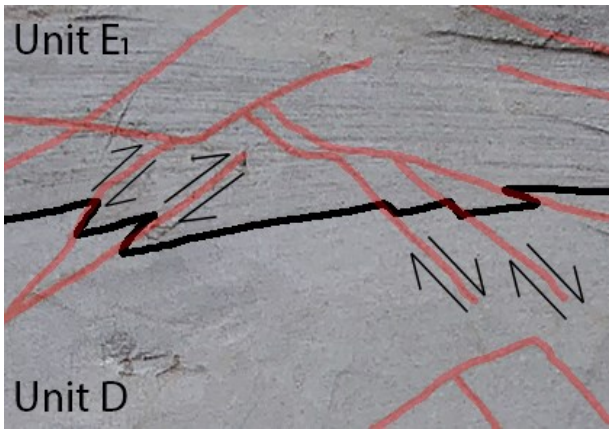

Figure 15. Close up from Figure 10 displaying section A and the contact between unit D and unit E1. The contact displays the visual characteristics of one or a series of box folds, but no distortion of the horizontal lamination closest to the contact.

displays the same kind of horizontal lamination and reverse faults as unit B, with the addition of a single reverse fault cutting through the unit at a right angle of the other reverse faults. The reverse faults present in the previous unit D continues upwards unhindered into and through unit E1. Three fault planes were measured of which two align closely and the third is to a large extent oriented in the opposite direction (Fig. 13). The lower contact towards the previous unit D is sharp and has the visual characteristics of a box fold (Fig. 15), but with no distortion of the lamination toward the contact. The contact plane was measured and appears seemingly flat with little to no dip.

Subunit E2. Subunit E2 is the lateral continuation to the left of unit E1 and the unit thickness of the subunit is here 95 cm (Fig. 12; Fig. 13). Unit E2 exhibits the same general characteristics as unit E1 (Sh), with the exception that the contact with unit C at the bottom of unit E2, the contact plane was unfortunately not measured. Unit E2 is dissected by the same reverse kind of reverse faults observed in E1 and a total of four fault planes were measured with shallow dips between 8–24° towards a general dip azimuth of NNE (Fig. 13). Towards the top of unit E2 a thin fracture 1–3 cm thick with massive sediments is visible at an apparent right angle of the other reverse faults in the unit.

Subunit Unit E3. Subunit E3 is the vertical continuation and situated just above unit E2 and the sub unit is 35 cm thick with the upper contact disappearing above the exposure (Fig. 12; Fig. 13). Unit E3 exhibits the same general characteristics as unit E1 and E2 (Sh). A single fault plane was measured with a dip of 22° toward azimuth of 200° SSW.

4.2.2 Section A – interpretation

Five major units, one composed of three subunits, were previously described in 4.2.1. Several of the units are interpreted to originally belong to the same unit, but to have likely been affected by post-depositional processes to result in their current shapes and order. Units A and D are similar to the extent that the only real differences found are determined to originate from post-depositional processes, and unit A and D are therefore considered the same unit in regards to primary deposition. This holds true for unit B and E as well, which will also be considered the same unit with respect to their primary deposition.

Unit A and D. The well-sorted composition, fine lamination and lack of clasts in these units indicate fluvial sorting and deposition in a proglacial environment (Benn & Evans 2010). The sediment has in turn been deformed, as observed by the abundance of reverse faults that can be found throughout the unit, but show no signs of shearing. This deformation has occurred post-depositionally as the faults cross-cut the fine depositional laminae of the sand. This leads to the deduction that the sediment units were originally glaciolacustrine sand deposited in a proglacial environment, likely a basin, and then later pushed up by a nearby ice sheet margin, causing lateral compression. The units are therefore interpreted as glaciolacustrine sand turned into type B glacitectonite (Benn & Evans 1996; Benn & Evans 2010; Evans & Benn 2021) most likely associated with proglacial push (Hart & Boulton 1991).

Unit B and E. These units, much like the previous unit A and, also consist of well-sorted sand with fine lamination. The laminae are darker and slightly denser, but the grain sizes present are indistinguishable from units A and D. This similarity indicates fluvial sorting and deposition in a proglacial environment as well (Benn & Evans 2010). Several deformation structures in the form of reverse faults are also found, with the addition that bifurcation of the faults is commonly observed. This deformation has also occurred through a process that occurred after primary deposition, as the faults are observed crossing the fine laminae of the sand. This leads to the conclusion that the primary deposition of both units B and E were as glaciolacustrine sand deposited in a proglacial basin. This sediment pile later experienced pushing of a nearby ice sheet margin causing lateral compression and the creation of the current ridge that is composed of these sediments. The units are therefore interpreted as glaciolacustrine sand turned into type B glacitectonite (Benn & Evans 1996; Benn & Evans 2010;

Evans & Benn 2021).

Unit C. This thin unit consists of sand that is well-sorted and massive in structure. Along its length several water-injection features are observed (Fig. 16) (Phillips et al. 2013), but no displacement or faulting of the sediments was found. The presence of these structures indicates that the area is likely to have been subjected to an increase in pore water pressure, which is likely to happen proximal to the margin of an ice sheet, or in a submarginal environment (Phillips et al. 2013; Ravier & Buoncristiani 2018). These conditions forced water and sediment to be injected into and between surrounding units. Unit C is therefore interpreted to be a water-injected sand that is part of a more extensive water-injection structure or hydrofracture fill (Phillips et al. 2013).

Genesis. Unit A and D were originally one unit, based on the clear marker horizons in each unit that continue in the other, now called unit AD. Together they formed a sorted glaciolacustrine sand with horizontal fine lamination. Similarly unit B and E were also originally one unit, now called unit BE. They were also made up of a sorted glaciolacustrine sand, with the addition that the darker laminae present hint toward having formed at a slightly different depositional environment, as the material content is slightly different compared to unit AD (Fig. 12). Unit AD and BE were both formed in a proglacial environment, likely a basin in front of an ice-margin (Benn & Evans 1996; Benn & Evans 2010; Evans & Benn 2021). As the ice-margin at a later stage of the glaciation readvances, both of the sediment units AD and BE were pushed by the ice, which in turn displaced them into and on top of each other, causing them to interfinger on a large scale of at least several meters in height (Fig. 12). Due to the scale of the interfingering in relation to the section, it is not possible to deduce a relative age or stratigraphy for units AD and BE, or which one has been displaced the most; for this, more extensive exposure conditions would be required, which was not possible at this site. The reverse faults in both AD and BE can be traced across unit contacts (Fig. 13), and must therefore postdate shearing and interfingering. At some point the pore water pressure increases at the contact between unit B and D. Water is then forcibly injected between unit B and D, causing the overlying sediment units to lift through a hydraulic jack as the pore pressure increases, while simultaneously injecting sediments (Fig. 12; Fig. 16) (Phillips et al. 2013; Ravier & Buoncristiani 2018). The water-injected sand (unit C) cut through the previous reverse faults but causes little to no displacement as most of them are still traceable from unit B into unit D, with unit C acting as a separator with regards to the fault planes (Fig. 16) Whether or how far the ice retreated between the interfingering of units AD and BE and water injection cannot be ascertained at this stage and requires further investigation.

4.2.3 Section B – description

Section B is located in an old, abandoned gravel and sandpit on the southern side of a 480 m long and 200 m wide landform in the northern part of the study area (N55.5836°, E13.7314°; Fig. 6). The hummock has a slight parabolic shape but the overall orientation extends from 260° W to 80° E. An exposure 2 m wide and 1 m high was cleared with an orientation of 330° NNW to 150° SSE (left to right) on the northern side of the sandpit close to the top. A mosaic was constructed (Fig. 17) using three detailed photos of the exposure and used as the base for a digitalised 2d-log (Fig. 18). The exposure was divided into two major units, labelled A and B from the bottom and counting upwards.

Unit A. The lowermost unit in the cleared exposure is at least 100 cm thick with the lower contact disappearing beneath the exposure (Fig. 18), likely for several meters as observed in other shallow exposures around the pit. The unit consists mainly of a dark brown, clast-supported gravel with some imbrication or stacking of clasts, while also containing several outsized clasts. The matrix is between 2–5 mm in

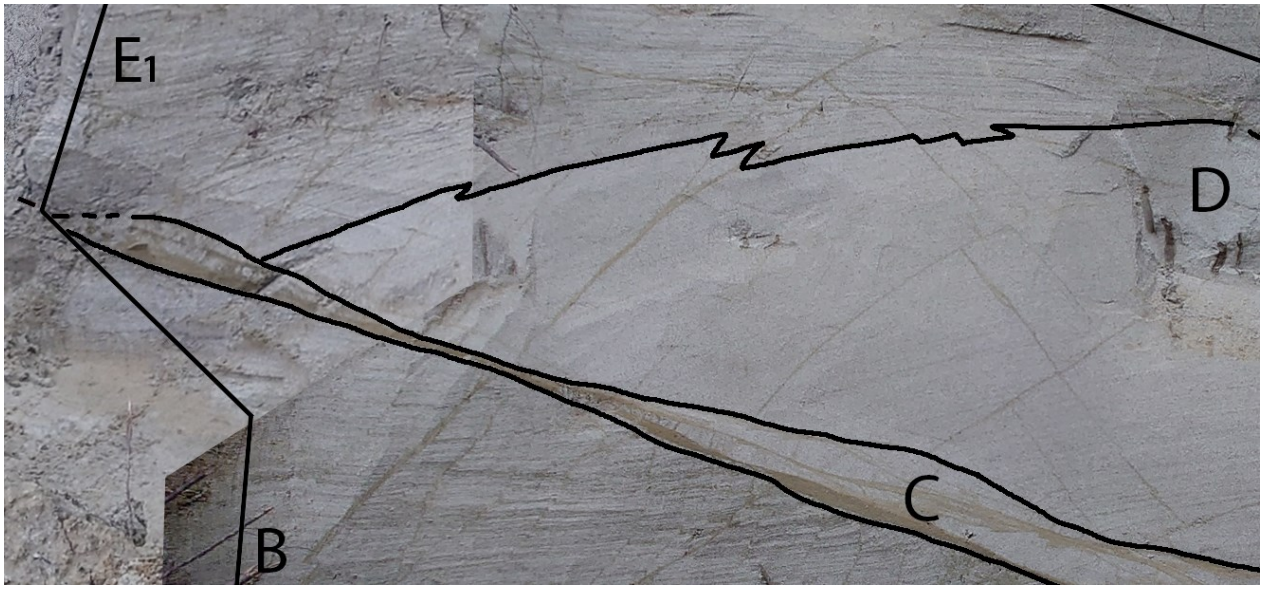

Figure 16. Close up from Figure 10. Unit C is interpreted to be water-injected sediments post deposition and post deformation of unit B and D.

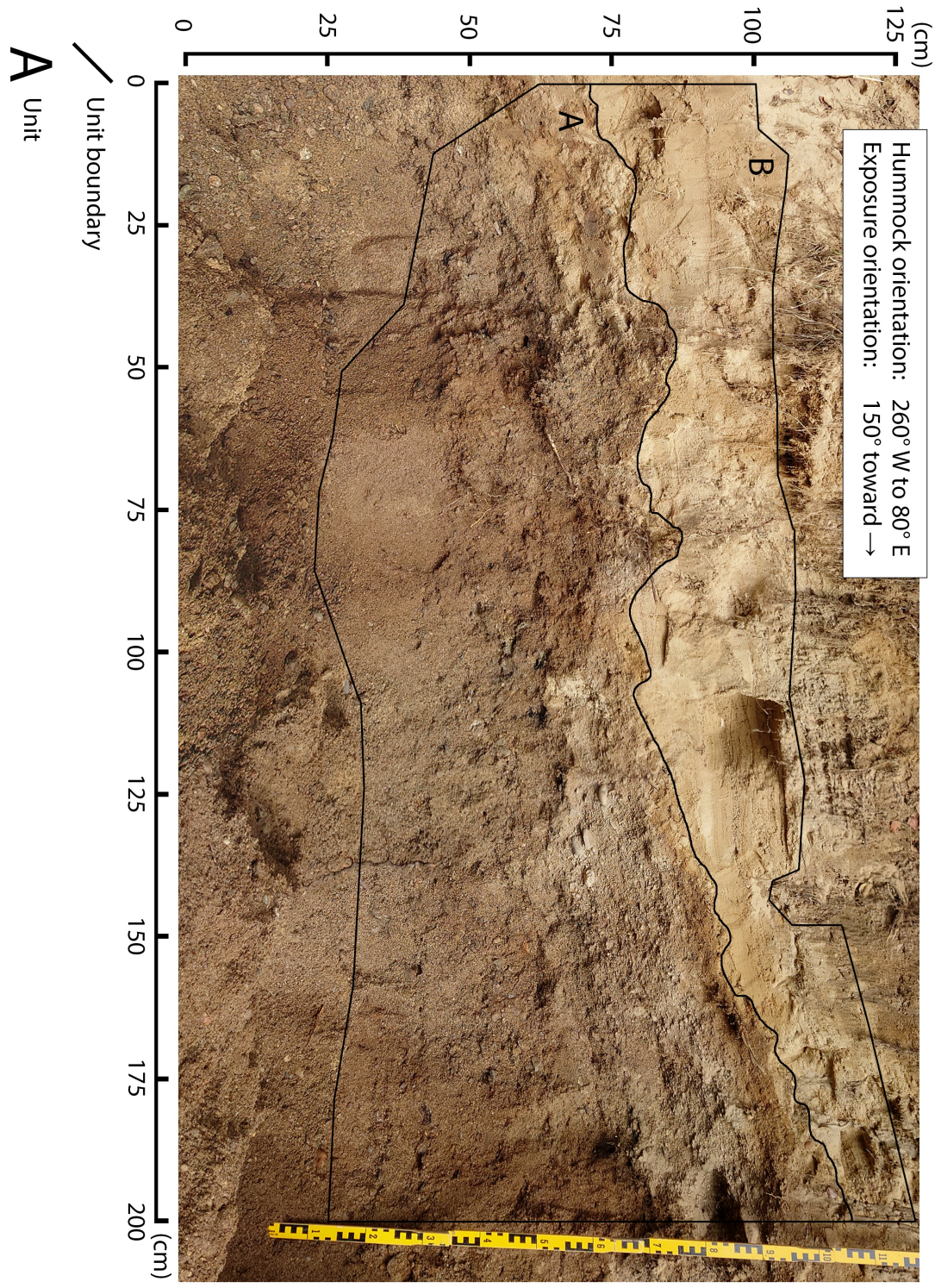

Figure 17. Mosaic constructed from three detailed photos showing the exposure of section B. The exposure is 2 m wide and 1 m tall and is divided into two major units. Unit A is made up of mainly gravel with some imbrication of clasts, and unit B is made up of mainly sand with some streaks and lenses of fine granules.

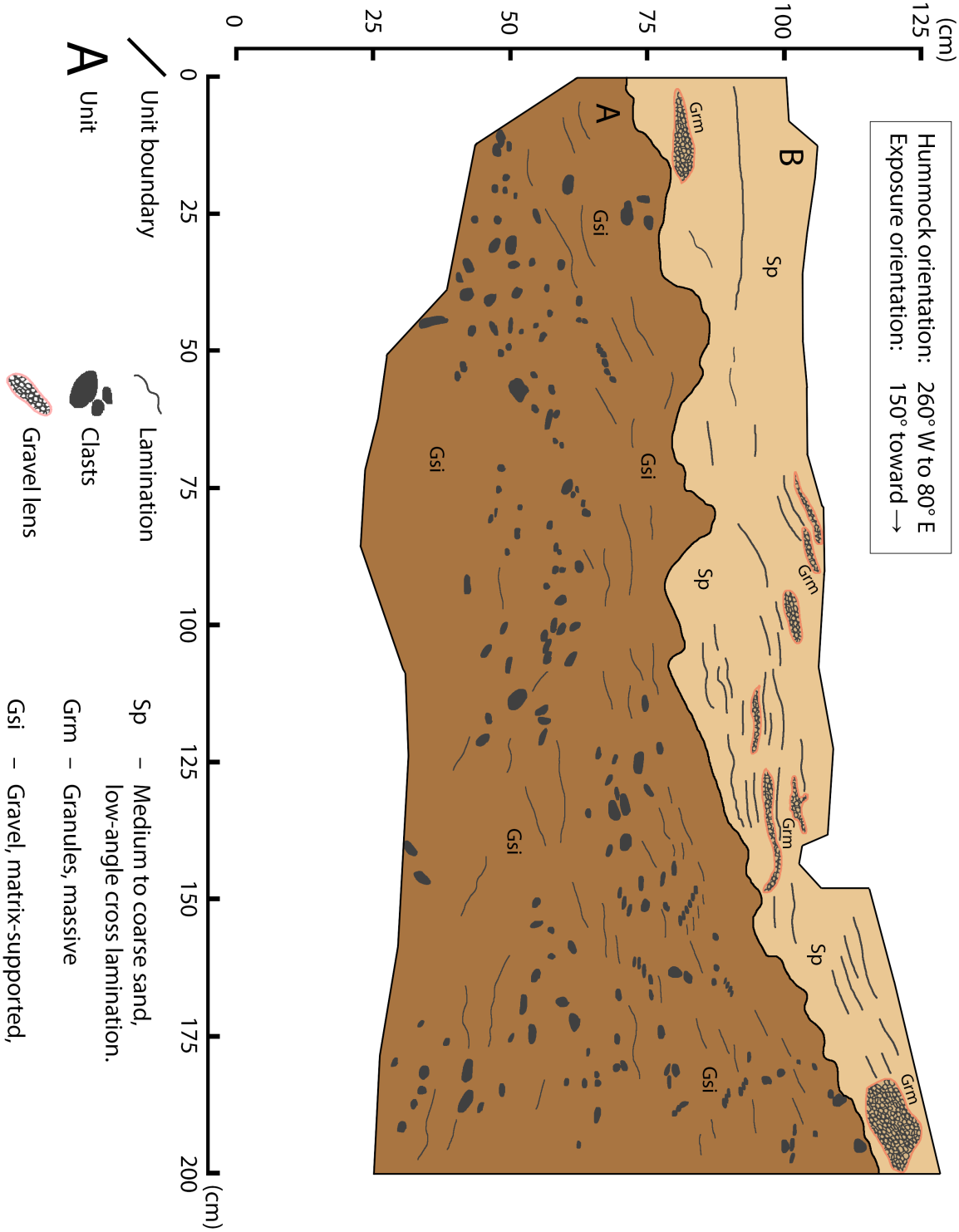

Figure 18. 2d-log of the exposure in section B, as also seen in Figure 16. Lithofacies codes are based on the methodology of Benn & Evans (2010) and Evans & Benn (2021).

grain size, and scattered with smaller clasts with maximum a-axes between 3–6 cm long. These clasts can often be found stacked throughout the entire unit (Fig. 19). Some outsized clasts up to around 10 cm were found, in which case they were most commonly matrix supported. Both the regular clasts and the outsized clasts were of different lithologies: more rounded clasts were predominately crystalline in nature, while more angular clasts were often found to be shale or chalk brittle to the touch. The unit shows vague lamination or bedding, seemingly aligning with the trend of the stacking and/or imbrication. Neither the lamination, stacking nor imbrication were successfully measured as the unconsolidated sediment fell apart at such attempts.

Unit B. This unit makes up the uppermost part of the exposure and is at least 50 cm thick with the upper contact intersecting the ground surface (Fig. 18). The unit consists of a medium to coarse sand in a light colour with a slight yellow tint. The sand contains lamination that is vague and poorly defined, and is best described as either a wavy sub-parallel lamination that is partially discontinuous cross lamination (Collinson & Mountney 2019). Ten measurements were taken of the lamination indicating a clear trend of the laminae dipping 20 ±8° toward azimuth 42 ±15° NE (Fig. 20). The contact plane between unit A and B is sharp and indicates a dip of 28 ±8° toward the dip azimuth 21 ±10° NNE based on five measurements (Fig. 20). This shows that the contact planes align fairly closely with the measured planes of the laminae in unit B. Scattered throughout the unit are several lenticular bodies commonly 10–30 cm long filled with fine granules 2–4 mm in grain size (Fig. 18). In addition to the lenticular bodies, thin and discontinuous streaks of the same granules are scattered throughout, following the same lamination as found in the dominating sand.

Figure 19. Close up from Figure 16, showing stacking of the gravel in unit A from section B.

2.1.1 Section B – interpretation

Two major units belonging to section B were previously described in 4.2.3 and are here interpreted.

Unit A. Due to the clast supported and mostly sorted sediments and vague lamination, this unit is interpreted to have formed in a fluvial proglacial environment (Benn & Evans 2010). The mostly mature clasts of crystalline origin are mixed in with more angular clasts of shale and chalk. The shale and chalk indicate a short journey of transportation as a longer one would quickly break them apart, while the mature crystalline clasts have in turn likely been part of previous glaciofluvial rounding and later been reworked into the current unit (Benn & Ballantyne 1994; Lukas et al. 2013). The observed imbrication could indicate a relatively high-energy environment with a unidirectional flow of water found in a glaciofluvial environment (Gough 2021), while the stacked clasts appear to be climbing on top of each other and are reminiscent of structures that can be found in delta foresets (Collinson & Mountney 2019). Due to the larger clasts and absence of any other lacustrine indications, Unit A is therefore interpreted as a glaciofluvial clast-supported gravel.

Unit B. In regards to the sorted sand and albeit vague lamination, this unit is interpreted to have formed in a fluvial proglacial environment (Benn & Evans 2010). The addition of both streaks- and lenticular lenses of granules among the sorted sand indicate a variation in water input, likely in the form of meltwater pulses from a not too distant ice-margin (Benn & Evans 2010). Unit B is therefore interpreted as a glaciofluvial deposit of sorted sand containing small amounts of granules in the form of thin streaks and lenses (Collinson & Mountney 2019).

Genesis. In the first stage of this section the lowermost unit A consisting of glaciofluvial gravel was deposited in a proglacial environment in close proximity to a retreating ice-margin. The sharp contact

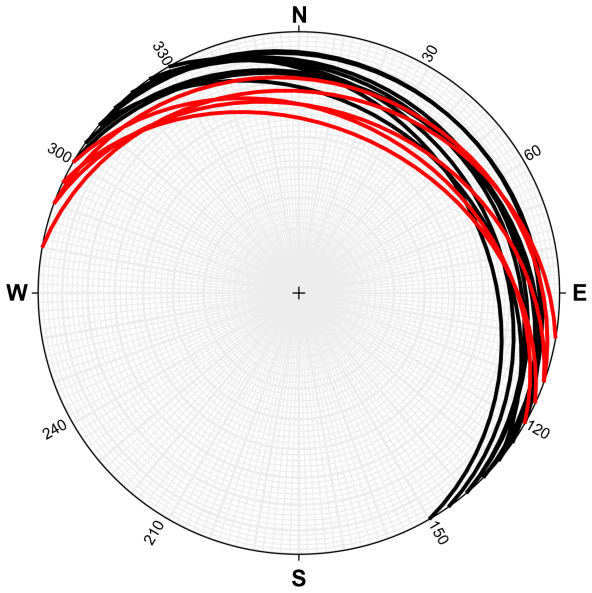

Figure 20. Stereonet showing five measurements of the contact between unit A and B (red), and ten measurements of the laminae (black) of unit B.

between the unit of gravel and overlaying unit of sorted sand indicate a sudden shift in fluvial energy levels. The sorted sand containing streaks and lenses of granules point toward a lower energy environment with periodic faster flows of water carrying granules with it. At this point the depositional environment is likely less proximal.

5 Discussion

By utilizing remote sensing analysis of the study area, and sedimentological analysis of associated landforms, a set of glacial features believed to originate from both active and stagnant ice has been identified in the landscape. In the following sections the interpretations and results presented above will be discussed.

5.1 Genesis of hummocky moraine

To ascertain the proper classification of hummocky moraine and its preconceived associated chaotic spatial component, it is important to map the orientation of several such assumed landforms. Contrary to previous assertions that there is no spatial order to the hummocky moraine landscape (Daniel 1986, 1992), the evidence inside the smaller ~35 km2 focus area strongly shows that there is a clear spatial relationship between the hummocks, ridges and depressions. All measurements of hummock orientation demonstrate that there are clear trends in the landscape with an orientation in a broad NW–SE direction (mean vector 133 ±5° and eigenvalue S1=0.6441 for all elongated hummocks). The ridges with similar orientation can often be linked together to form discontinuous chains through the landscape, with several such chains being parallel to one another. Crestlines on one hummock often find a correlative and continuation in a neighbouring hummock, strongly suggesting a far-from-random coincidence and thus orientation. Some crestlines are found staggered 25–50 m apart, similar to annual moraines (Chandler et al. 2020). Due to these findings, it is not out of the question to start forming a hypothesis and regard each discontinuous chain as a former paleo ice-margin, similar to the previous work of Benn (1992), Bennett (1994), Wilson & Evans (2000), Benn & Lukas (2006), and Lovell et al. (2018). In fact, the similarities of these relationships are striking. Not all mapped hummocks or ridges do conform with their orientation along a projected paleo ice-margin, and seldom can one follow a suggested chain of hummocks representing a paleo ice-margin more than 500 to 2000 m long (Lovell et al. 2018). Larger hummocks and larger composite landforms consisting of several inseparable hummocks, depicted in red in *Figure 9*, generally show tighter groupings with respect to their orientation as shown by the higher S1 eigenvalues, compared to the smaller hummocks less than 40 000 m2 in size shown in blue in the same figure. The smaller hummocks are slightly more chaotic in their orientation and spatial relation between each other, compared to the larger ones. Yet they still show clear trends in their orientation as seen in the stereonet projections (Fig. 10; Fig. 11). When combining and projecting the orientation of all 283 elongated hummocks regardless of size in a single stereonet projection (Fig. 11), a 95 % average indicate a mean vector of orientation toward 133 ±5° SE, with the majority of hummocks orientated in a direction between 90° E and 190° S. Special note should be taken that, while the majority of hummocks trend toward the southeast, there is a distinct lack of mapped elongated hummocks perpendicular to the vast majority of these (Fig. 11). This is strong geomorphological evidence that within the ~35 km2 focus area the hummocky landscape is far from chaotic.

In the whole of the ~80 km2 large study area 41 IWLPs are identified with varying degree of certainty (Table 2). IWLPs are remnants from the infillings of ice-walled lakes, and are often associated with stagnant or dead ice (Clayton et al. 2008). There is a stark contrast for the frequency and concentration of the IWLPs, with less than 20 % of the mapped IWLPs found inside the smaller ~35 km2 focus area, and 80 % found in the remainder of the larger study area (Fig. 9). It is therefore believed that outside the smaller focus area, and in the remainder of the larger study area, an extensive amount of dead ice was present across the region at a late stage of deglaciation. While it is worth mentioning, partial dead ice cut-off could occur during the retreat of the ice-margin (Eyles 1983), but this would have to be investigated further to be ascertained.

Two hummocks were selected for sedimentological analysis to get a better understanding of the internal composition of the hummocks and to gain more insights into their genesis. Section A (described in results 4.2.1 and 4.2.2) contains exclusively sorted sand riddled with reverse faulting and interfingering of units on a large scale. The measured thrust fault planes and contacts are perpendicular to the orientation of this particular hummock (Fig. 13). These thrust faults are known to develop parallel to shear planes and perpendicular to the direction of ice-flow (Aber et al. 1989; Benn & Evans 2010). The ca. 30° thrust angle of the planes is reminiscent of overthrust faults. Since continued lateral compression in a proglacial environment by an advancing ice-margin can cause the development of multiple thrust sequences (Benn & Evans 2010), and in the absence of other processes that could have caused such compression, proglacial glaciotectonism is interpreted to be the most likely cause of deformation. Some of the thrust fault planes dip in the opposite direction (Fig. 13), likely due to layer-parallel compression causing back thrusts (Benn & Evans 2010). There are also small traces of anastomosing fault patterns, yet another evidence for proglacial compression (Benn & Evans 2010). An advancing or oscillating ice sheet pushing against proglacial sediments can cause both folding and thrust faulting to occur hundreds of meters from the ice-margin (Lovell et al. 2018). It is therefore most likely that the sediments in section A were subjected to lateral compression through proglacial pushing which caused the reverse faulting to occur.

Section B (described in results 4.2.3 and 4.2.4) contains two units with large differences and a clear contact in between (Fig. 18). One unit is a clast supported glaciofluvial gravel and the second unit is made up of glaciofluvial sand with streaks of granules. Most notably there is a complete lack of deformation structures in these two units of section B. Comparing

the sediments found in section A with section B, they indicate different primary depositional environments. Section A indicate a glaciolacustrine environment while section B indicate a more proximal glaciofluvial environment, yet the outwards appearance and shape of the hummocks in which the sediments are found are roughly the same. The contact planes and laminae in section B coincide fairly closely with the directional element of the fault planes of section A, while clearly having no other association with deformation structures or lateral compression.

While section A and section B tell slightly different stories of origin, one based on glaciolacustrine and one based on glaciofluvial deposition, other sediments have also previously been observed in the study area. Amongst these we find both glacial till and glaciolacustrine clay as parts of the hummocks (Munthe 1920; Daniel 1986; Lidmar-Bergström et al. 1991; Daniel 1992), and from wells and boreholes multiple layers of till have been observed with inter till layers of various sediments like sands and gravels (Munthe 1920; Daniel 1986; Lidmar-Bergström et al. 1991; Daniel 1992). This indicate that at least parts of the study area were overridden by the ice sheet more than once, depositing new sediment on top of older preserved layers. These tills are often described as rich in clay that has been picked up from surrounding shale in the region (Lidmar-Bergström et al. 1991; Daniel 1992), and often found glaciofluvially reworked into clay-rich gravel (Daniel 1986, 1992).

5.2 Implications of findings for former models of ice retreat and dynamics.

Putting together the results and findings of this thesis, the evidence helps to add and improve on the observations of Daniel (1986, 1992) and the deglaciation model of Scania by Lidmar-Bergström et al. (1991) (Fig. 4). While it is not the focus of this thesis to discuss specific ages for deglaciation, some of them are relevant for the study area as they correlate with known deglaciation events.

During the deglaciation of Scania the study area started to become ice-free ca 18–15 ka (Lidmar-Bergström et al. 1991; Ringberg 2003). Deglaciation has generally been deemed to occur from the west toward the east (Lidmar-Bergström et al. 1991; Houmark-Nielsen & Kjær 2003; Stroeven et al. 2016), while an active ice-margin has been fed and supplied with ice from the Lower Baltic ice stream (Ringberg 2003; Szuman et al. 2021). As a large block of dead ice was deposited over southern Scania as seen in *Figure 4*, which was estimated to be about 50 km long and between 10–15 km wide (Lidmar-Bergström et al. 1991), the Lower Baltic ice stream continued to feed the eastward-retreating ice-margin to the north of the dead ice, while simultaneously going around to the south of the dead ice and circumventing it before turning northwards (Fig. 21). The inferred position and/or size of the block of dead ice by Lidmar-Bergström et al. (1991) match quite well with the eastern to southern parts of the study area which have a higher frequency of IWLPs present which support the idea of a vast dead ice covering the region. This also aligns with the views of Daniel (1986, 1992). This block of dead ice is suggested to have a large overlap with the smaller focus area, which contradicts some of the findings in this thesis.

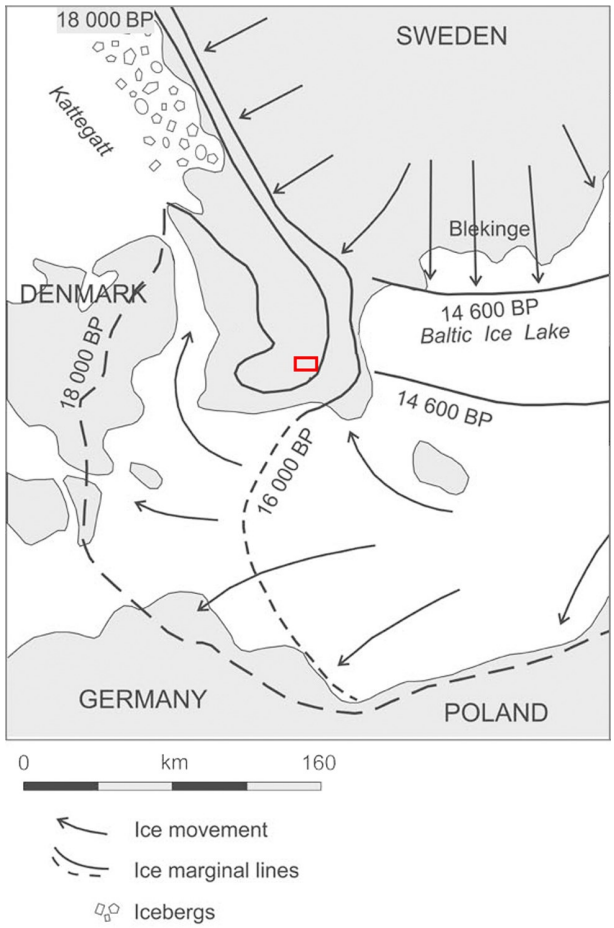

Figure 21. Map over southern Sweden with study area marked with a red rectangle. According to this model central Scania was ice-free ca. 18 ka in the shape of an inverted lobe, but still covered in ice in and around the edges of Scania. The arrows in the Baltic Ice Lake indicate ice movement and representing the movement of the Lower Baltic ice stream, which continued to feed and supply the ice-sheet in southern Scania with ice. Modified from Ringberg (2003).

The sedimentological analysis of section A show evidence of the sediments having been affected by an active ice-margin, as per the deformation structures observed. As the thrust faults of section A align perpendicular to the orientation of the very same hummock they are found in, and are closely associated with proglacial push, this could very well mark the position of a temporary advance or oscillation of the paleo ice-margin during overall net retreat. This directly contradicts the idea of large bodies of dead ice being cut off from the ice sheet margin that are then left to melt out passively or being occupied by the Vomb Ice Lake. Unfortunately there is not sufficient knowledge to interpret the dynamic state of the ice margin at the time of hummock formation at this stage, but that the side-by-side presence of actively-retreating and/or oscillating margins, and zones of dead ice being cut off between moraines/ice-marginal positions, may point to a more active margin. There could potentially be isolated and localised areas of ice stagnation and

dead ice undergoing downwasting at the same time (Eyles 1983), as left behind by the retreating ice-margin.

5.3 Suggested complementary research

The deglaciation history of Scania is often overlooked or simplified in the established literature related to the deglaciation of southern Fennoscandia (Lundqvist & Wohlfarth 2000; Houmark-Nielsen & Kjær 2003; Anjar et al. 2014; Stroeven et al. 2016; Patton et al. 2017; Möller et al. 2019). This is most likely due to the severe complexity of the course of events that took place and the difficulties in piecing together a single coherent deglaciation sequence (including re- advances) of the region. West of the mapped area and Romeleåsen, a vast landscape previously determined as hummocky moraine is said to originate from the same block of dead ice spreads out from Ystad toward Malmö (Lidmar-Bergström et al. 1991; Daniel 1992), and could potentially benefit from a fresh inventory of the glacial components. The geomorphological complexity of the region could benefit from mapping and categorising one typical area at a time to steadily improve and build upon a more detailed model for the deglaciation of Scania.

7 Conclusions

- LiDAR data covering a ~80 km2 large study area has been used to remotely map the landforms of an area previously classified as 'hummocky moraine'. By gathering remote data related to foremost directional elements for a total of 41 ice-walled lake plains, 367 hummocks, and 691 associated crestlines; and combining these with sedimentological evidence gathered in the field from two exposures, insight has been gained in the trends and genesis of the landscape.
- Sedimentological evidence strongly suggest that glaciolacustrine sediments have been subjected to lateral compression perpendicular to the hummock orientation, which is most often associated with proglacial push.
- The hummocks within the smaller focus area indicate little to no evidence for large scale stagnation as previously suggested by Lidmar-Bergström et al. (1991) and Daniel (1992).
- The hummocks and clay plateaus in the larger study area show strong indication of largescale widespread stagnation and downwasting as previously suggested by Lidmar-Bergström et al. (1991) and Daniel (1992).
- Based on the geomorphological and sedimentological evidence, the hummocky moraine in the study area is interpreted to not have solely formed by ice sheet stagnation and downwasting of dead ice, but instead been linked to processes of both active and stagnant ice.
- Due to the spatial order and preservation of the hummocks as well as their sedimentological content, it has been demonstrated that the term hummocky moraine is too broad and terminologically loaded with dead ice meltout or 'passive' deglaciation. Alternative and more descriptive terminology and classifications such as hummocky- or undulating terrain could in some cases be more suitable when the landforms have yet to be properly classified.

7 Acknowledgements

The These acknowledgements are for more than just help and support toward me with my thesis, but for having a significant impact and having influenced me as a person during these past years I have spent as a student at Lund University.

Sven Lukas, thank you for being my supervisor. Thank you for your expertise, encouragement, enthusiasm and understanding since the first time I set my foot in your classroom. I am proud to consider you my friend.

Helena Alexanderson, thank you for being my first and most important inspiration to pursue Quaternary geology. Without you I might have turned out to be another bedrock geologist like so many others, but thanks to your lectures I was inspired to become something much cooler.

Emmy Molin, you are outright amazing. Thank you for being my classmate, friend and confidant these past six years. I could never wish for a better study-buddy, nor partner in crime.

8 References

Aario, R. (1977). Classification and terminology of morainic landforms in Finland. *Boreas, 6*(2), 87-100. doi: 10.1111/j.1502-3885.1977.tb00338.x

Aber, J. S., Croot, D. G., & Fenton, M. M. (1989). *Glaciotectonic landforms and structures*. Kluwer, Dordrecht. doi: 10.1002/jqs.3390050309

Allmendinger, R. W., Cardozo, N., & Fisher, D. (2012). *Structural geology algorithms: Vectors and tensors in structural geology*. Cambridge University Press. doi: 10.1017/CBO9780511920202

Anjar, J. (2012). *The Weichselian in southern Sweden and southwestern Baltic Sea : glacial stratigraphy, palaeoenvironments and deglaciation chronology* [Theses, Quaternary Sciences, Department of Geology, Lund University].

Anjar, J., Adrielsson, L., Larsen, N., Möller, P., & Barth, K. (2014). Weichselian history of the Fennoscandian ice sheet in southern Sweden and the southwestern Baltic Basin. *Boreas, 43*. doi: 10.1111/bor.12048

Benn, D. I. (1992). The genesis and significance of 'hummocky moraine': Evidence from the Isle of Skye, Scotland. *Quaternary Science Reviews, 11*(7), 781-799. doi: 10.1016/0277-3791(92)90083-K

Benn, D. I., & Ballantyne, C. K. (1994). Recon-

structing the transport history of glacigenic sediments: a new approach based on the covariance of clast form indices. *Sedimentary Geology, 91*(1), 215-227. doi: 10.1016/0037-0738(94)90130-9

Benn, D. I., & Evans, D. J. A. (1996). The interpretation and classification of subglacially-deformed materials. *Quaternary Science Reviews, 15*(1), 23-52. doi: 10.1016/0277-3791(95)00082-8

Benn, D. I., & Evans, D. J. A. (2010). *Glaciers and Glaciation* (2nd ed.). Hodder Education. doi: 10.4324/9780203785010

Benn, D. I., & Lukas, S. (2006). Younger Dryas glacial landsystems in North West Scotland: an assessment of modern analogues and palaeoclimatic implications. *Quaternary Science Reviews, 25*(17), 2390-2408. doi: 10.1016/j.quascirev.2006.02.015

Bennett, M. R. (1994). Morphological evidence as a guide to deglaciation following the Loch Lomond Readvance: A review of research approaches and models. *Scottish Geographical Magazine, 110*(1), 24-32. doi: 10.1080/00369229418736904

Bennett, M. R., & Boulton, G. S. (1993). A reinterpretation of Scottish 'hummocky moraine' and its significance for the deglaciation of the Scottish Highlands during the Younger Dryas or Loch Lomond Stadial. *Geological Magazine, 130*(3), 301-318. doi: 10.1017/S0016756800019993

Berglund, B. E., & Lagerlund, E. (1981). Eemian and Weichselian stratigraphy in South Sweden. *Boreas, 10*, 323–362. doi: 10.1111/j.1502-3885.1981.tb00494.x

Bergsten, K. E. (1981). Isälvsdalar i sydvästskåne. *Svensk Geografisk Årsbok, 57*, 19–24.

Cardozo, N., & Allmendinger, R. W. (2013). Spherical projections with OSXStereonet: Computers & Geosciences. doi: 10.1016/j.cageo.2012.07.021

Chandler, B. M. P., Chandler, S. J. P., Evans, D. J. A., Ewertowski, M. W., Lovell, H., Roberts, D. H., Schaefer, M., & Tomczyk, A. M. (2020). Sub-annual moraine formation at an active temperate Icelandic glacier. *Earth Surface Processes and Landforms, 45*(7), 1622-1643. doi: 10.1002/esp.4835

Chandler, B. M. P., Lovell, H., Boston, C. M., Lukas, S., Barr, I. D., Benediktsson, Í. Ö., Benn, D. I., Clark, C. D., Darvill, C. M., Evans, D. J. A., Ewertowski, M. W., Loibl, D., Margold, M., Otto, J.-C., Roberts, D. H., Stokes, C. R., Storrar, R. D., & Stroeven, A. P. (2018). Glacial geomorphological mapping: A review of approaches and frameworks for best practice. *Earth-Science Reviews, 185*, 806-846. doi: 10.1016/j.earscirev.2018.07.015

Clayton, L., Attig, J. W., Ham, N. R., Johnson, M. D., Jennings, C. E., & Syverson, K. M. (2008). Ice-walled-lake plains: Implications for the origin of hummocky glacial topography in middle North America. *Geomorphology, 97*(1), 237-248. doi: 10.1016/j.geomorph.2007.02.045

Cohen, K. M., & Gibbard, P. L. (2019). Global chronostratigraphical correlation table for the last 2.7 million years, version 2019 QI-500. *Quaternary International, 500*, 20-31. doi: 10.1016/j.quaint.2019.03.009

Collinson, J., & Mountney, N. (2019). *Sedimentary structures*. Dunedin Academic Press. doi: 10.4236/ojm.2012.23004

Daniel, E. (1986). *Ae 65 Beskrivning till jordartskartan 2D Tomelilla SO/2E Simrishamn SV*. SGU.

Daniel, E. (1992). *Ae 99 Beskrivning till jordartskartan 2D Tomelilla SV*. SGU.

Dowling, T., Alexanderson, H., & Möller, P. (2013, 06/01). The new high resolution LiDAR digital height model ('Ny Nationell Höjdmodell') and its application to Swedish Quaternary geomorphology. *GFF*. doi: 10.1080/11035897.2012.759269

Erlström, M., Sivhed, U., Wikman, H., & Kornfält, K.-A. (2004). *Af 212–214 Beskrivning till berggrundskartorna 2D Tomelilla NV, NO, SV, SO, 2E Simrishamn NV, SV, 1D Ystad NV, NO, 1E Örnahusen NV*. SGU.

Evans, D. J. A., & Benn, D. I. (2021). *A Practical Guide to the Study of Glacial Sediments* (2nd ed.). Routledge.

Eyles, N. (1983). Modern Icelandic glaciers as depositional models for 'hummocky moraine' in the Scottish Highlands. In *Evenson, E.B., Schliichter, C. and Rabassa, J. (eds), Tills and Related Deposits* (pp. 47–60). Balkema.

Gough, A. (2021). Sedimentary Structures. In D. Alderton & S. A. Elias (Eds.), *Encyclopedia of Geology (Second Edition)* (pp. 787-808). Academic Press. doi: 10.1016/B978-0-12-409548-9.11996-7

Gravenor, C. P., & Kupsch, W. O. (1959). Ice-Disintegration Features in Western Canada. *The Journal of Geology, 67*(1), 48-64. doi: 10.1086/626557

Gustafsson, O. (1969). Isströmmar över Sydskåne [Unpublished manuscript]. *Department of Geology, Lund University*.

Hart, J. K., & Boulton, G. S. (1991). The interrelation of glaciotectonic and glaciodepositional processes within the glacial environment. *Quaternary Science Reviews, 10*(4), 335-350. doi: 10.1016/0277-3791(91)90035-S

Hoppe, G. (1952). Hummocky Moraine Regions with Special Reference to the Interior of Norrbotten. *Geografiska Annaler, 34*(1-2), 1-72. doi: 10.1080/20014422.1952.11904365

Houmark-Nielsen, M. (2007). Extent and age of Middle and Late Pleistocene glaciations and periglacial episodes in Southern Jylland, Denmark. *Bulletin of the Geological Society of Denmark, 55*. doi: 10.37570/bgsd-2007-55-02

Houmark-Nielsen, M. (2010). Extent, age and dynamics of Marine Isotope Stage 3 glaciations in the southwestern Baltic Basin. *Boreas, 39*, 343-359. doi: 10.1111/j.1502-3885.2009.00136.x

Houmark-Nielsen, M., & Kjær, K. (2003). Southwest

Scandinavia, 40–15 kyr BP: palaeogeography and environmental change. *Journal of Quaternary Science, 18*(8), 769-786. doi: 10.1002/jqs.802

Hubbard, A., Bradwell, T., Golledge, N., Hall, A., Patton, H., Sugden, D., Cooper, R., & Stoker, M. (2009). Dynamic cycles, ice streams and their impact on the extent, chronology and deglaciation of the British-Irish Ice Sheet. *Quaternary Science Reviews, 28*, 758-776. doi: 10.1016/j.quascirev.2008.12.026

Hughes, A. L. C., Clark, C. D., & Jordan, C. J. (2010, 2010/01/01). Subglacial bedforms of the last British Ice Sheet. *Journal of Maps, 6*(1), 543-563. doi: 10.4113/jom.2010.1111

Hughes, A. L. C., Gyllencreutz, R., Lohne, Ø. S., Mangerud, J., & Svendsen, J. I. (2016). The last Eurasian ice sheets – a chronological database and time-slice reconstruction, DATED-1. *Boreas, 45*(1), 1-45. doi: 10.1111/bor.12142

Hörnsten, Å. (1979). *Maringeologiska kartan Helsingborg.* Uppsala, SGU.

Kjær, K., Houmark-Nielsen, M., & Richardt, N. (2003). Ice-flow patterns and dispersal of erratics at the southwestern margin of the last Scandinavian Ice Sheet. *Boreas, 32*, 130-148. doi: 10.1111/j.1502-3885.2003.tb01434.x

Lagerlund, E. (1980). Litostratigrafisk indelning av Västskånes Pleistocen och en ny glaciationsmodell för Weichsel. *LUNDQUA Report, 21*, 120.

Lantmäteriet. (2019). *Product description: GSD-Elevation data, Grid 2+. Version 2.5*.

Lantmäteriet. (2020). *GSD-Höjddata grid 2+ [DATASET]*.

Lidmar-Bergström, K., Elvhage, C., & Ringberg, B. (1991). Landforms in Skåne, South Sweden. *Geografiska Annaler: Series A, Physical Geography, 73*(2), 61-91. doi: 10.1080/04353676.1991.11880333

Lindberg Skutsjö, L. (2021). *Geologiska och hydrogeologiska tolkningar av SkyTEM-data från Vombsänkan, Sjöbo kommun, Skåne.* [Bsc thesis, Lund University]. Lund University Student Papers. http://lup.lub.lu.se/student-papers/record/9043463

Lindström, M., Lundqvist, J., Lundqvist, T., Sivhed, U., & Calner, M. (2011). *Sveriges geologi från urtid till nutid* (3rd ed.). Studentlitteratur.

Lovell, H., Benn, D. I., Lukas, S., Spagnolo, M., Cook, S. J., Swift, D. A., Clark, C. D., Yde, J. C., & Watts, T. (2018). Geomorphological investigation of multiphase glacitectonic composite ridge systems in Svalbard. *Geomorphology, 300*, 176-188. doi: 10.1016/j.geomorph.2017.10.024

Lukas, S. (2003). The moraines around the pass of Drumochter. *Scottish Geographical Journal, 119*(4), 383-393. doi: 10.1080/00369220318737185

Lukas, S., Benn, D. I., Boston, C. M., Brook, M., Coray, S., Evans, D. J. A., Graf, A., Kellerer-Pirklbauer, A., Kirkbride, M. P., Krabbendam, M., Lovell, H., Machiedo, M., Mills, S. C., Nye, K., Reinardy, B. T. I., Ross, F. H., & Signer, M. (2013). Clast shape analysis and clast transport paths in glacial environments: A critical review of methods and the role of lithology. *Earth-Science Reviews, 121*, 96-116. doi: 10.1016/j.earscirev.2013.02.005

Lundqvist, J., & Wohlfarth, B. (2000). Timing and east–west correlation of south Swedish ice marginal lines during the Late Weichselian. *Quaternary Science Reviews, 20*, 1127-1148. doi: 10.1016/S0277-3791(00)00142-6

Margold, M., & Jansson, K. (2012). Evaluation of data sources for mapping glacial meltwater features. *International Journal of Remote Sensing, 33*, 2355-2377. doi: 10.1080/01431161.2011.608738

Munthe, H. (1920). *Aa 142 Jordlagren i beskrivningen till kartbladet Sövdeborg*. SGU.

Möller, P. (2010). Melt-out till and ribbed moraine formation, a case study from south Sweden. *Sedimentary Geology, 232*, 161-180. doi: 10.1016/j.sedgeo.2009.11.003

Möller, P., Alexanderson, H., Anjar, J., & Björck, S. (2019). MIS 3 sediment stratigraphy in southern Sweden sheds new light on the complex glacial history and dynamics across southern Scandinavia. *Boreas*. doi: 10.1111/bor.12433

Nelson, H. (1949). *Simrishamn omland. Naturlandskapet, näringslivet och bebyggelsen*. AB Ehrnberg & Sons Läderfabrik.

Nilsson, P. (2013). *Grundvattenundersökningar i Skåne, Transient Elektromagnetisk Sondering.* [Msc thesis, Lunds Tekniska Högskola].

Patton, H., Hubbard, A., Andreassen, K., Auriac, A., Whitehouse, P. L., Stroeven, A. P., Shackleton, C., Winsborrow, M., Heyman, J., & Hall, A. M. (2017). Deglaciation of the Eurasian ice sheet complex. *Quaternary Science Reviews, 169*, 148-172. doi: 10.1016/j.quascirev.2017.05.019

Peterson, G., Johnson, M. D., & Smith, C. A. (2017). Glacial geomorphology of the south Swedish uplands – focus on the spatial distribution of hummock tracts. *Journal of Maps, 13*(2), 534-544. doi: 10.1080/17445647.2017.1336121

Phillips, E., Everest, J., & Reeves, H. (2013). Micromorphological evidence for subglacial multiphase sedimentation and deformation during overpressurized fluid flow associated with hydrofracturing. *Boreas, 42*(2), 395-427. doi: 10.1111/j.1502-3885.2012.00261.x

Ravier, E., & Buoncristiani, J.-F. (2018). Glaciohydrogeology. In (pp. 431-466). doi: 10.1016/B978-0-08-100524-8.00013-0

Ringberg, B. (2003). Readvance and retreat of the Late Weichselian Low Baltic ice stream in southernmost Sweden – a review. *GFF 125*(3), 169-176. doi: 10.1080/11035890301253169

SGU. (1985). *Ae 65 Jordartskartan 2D Tomelilla SO/2E Simrishamn SV*. Uppsala, SGU.

SGU. (1989). *Ae 99 Jordartskartan 2D Tomelilla SV*. Uppsala, SGU.

SGU. (2005). *Af 214 Berggrundskartan 2D Tomelilla SV & 1D Ystad NV*. Uppsala, SGU.

SGU. (2014). *JORDARTER 1:25000-1:100000 [DATASET]*.

SGU. (2015). *Högsta Kustlinjen [DATASET]* Version 1).

SGU. (2022). *SGUs kartvisare JORDARTER 1:25000-1:100000* [Map]. https://apps.sgu.se/kartvisare/kartvisare-jordarter-25-100.html

Smith, M., & Clark, C. (2005). Methods for the visualization of digital elevation models for landform mapping. *Earth Surface Processes and Landforms, 30*. doi: 10.1002/esp.1210

Stroeven, A. P., Hättestrand, C., Kleman, J., Heyman, J., Fabel, D., Fredin, O., Goodfellow, B. W., Harbor, J. M., Jansen, J. D., Olsen, L., Caffee, M. W., Fink, D., Lundqvist, J., Rosqvist, G. C., Strömberg, B., & Jansson, K. N. (2016). Deglaciation of Fennoscandia. *Quaternary Science Reviews, 147*, 91-121. doi: 10.1016/j.quascirev.2015.09.016

Sundberg, S. B. (2000). *Sedimentprocesser och avlagringar för kantrygg kring platåleran vid Rydsgårds gods i backlandskapet söder om Romeleåsen, Skåne* [Thesis, Lund University]. Lund University Student Papers. http://lup.lub.lu.se/student-papers/record/2343941

Szuman, I., Kalita, J. Z., Ewertowski, M. W., Clark, C. D., Livingstone, S. J., & Kasprzak, L. (2021). GIS dataset: geomorphological record of terrestrial-terminating ice streams, southern sector of the Baltic Ice Stream Complex, last Scandinavian Ice Sheet, Poland. *Earth Syst. Sci. Data, 13*(10), 4635-4651. doi: 10.5194/essd-13-4635-2021

Westergard, A. H. (1906). *Platålera, en supramarin hvarfvig lera från Skåne*. Kungl. boktryckeriet, P.A. Norstedt & söner.

Wilson, S. B., & Evans, D. J. A. (2000). Coire a' Cheud-chnoic, the 'hummocky moraine' of Glen Torridon. *Scottish Geographical Journal, 116*(2), 149-158. doi: 10.1080/00369220018737088

Woodcock, N. H. (1977). Specification of fabric shapes using an eigenvalue method. *GSA Bulletin, 88*(9), 1231-1236. doi: 10.1130/0016-7606(1977)88%3C1231:SOFSUA%3E2.0.CO;2

Tidigare skrifter i serien ”Examensarbeten i Geologi vid Lunds universitet”:

588. Bejarano Arias, Ingrid, 2020: Determination of depositional environment and luminescence dating of Pleistocene deposits in the Biely Váh valley, southern foothills of the Tatra Mountains, Slovakia. (45 hp)
589. Olla, Daniel, 2020: Petrografisk beskrivning av Prekambriska ortognejser i den undre delen av Särvskollan, mellersta delen av Skollenheten, Kaledonska orogenen. (15 hp)
590. Friberg, Nils, 2020: Är den sydatlantiska magnetiska anomalin ett återkommande fenomen? (15 hp)
591. Brakebusch, Linus, 2020: Klimat och väder i Nordatlanten-regionen under det senaste årtusendet. (15 hp)
592. Boestam, Max, 2020: Stränder med erosion och ackumulation längs kuststräckan Trelleborg - Abbekås under perioden 2007-2018. (15 hp)
593. Agudelo Motta, Laura Catalina, 2020: Methods for rockfall risk assessment and estimation of runout zones: A case study in Gothenburg, SW Sweden. (45 hp)
594. Johansson, Jonna, 2020: Potentiella nedslagskratrar i Sverige med fokus på Östersjön och östkusten. (15 hp)
595. Haag, Vendela, 2020: Studying magmatic systems through chemical analyses on clinopyroxene - a look into the history of the Teno ankaramites, Tenerife. (45 hp)
596. Kryffin, Isidora, 2020: Kan benceller bevaras över miljontals år? (15 hp)
597. Halvarsson, Ellinor, 2020: Sökande efter nedslagskratrar i Sverige, med fokus på avtryck i berggrunden. (15 hp)
598. Jirdén, Elin, 2020: Kustprocesser i Arktis – med en fallstudie på Prins Karls Forland, Svalbard. (15 hp)
599. Chonewicz, Julia, 2020: The Eemian Baltic Sea hydrography and paleoenvironment based on foraminiferal geochemistry. (45 hp)
600. Paradeisis-Stathis, Savvas, 2020: Holocene lake-level changes in the Siljan Lake District – Towards validation of von Post’s drainage scenario. (45 hp)
601. Johansson, Adam, 2020: Groundwater flow modelling to address hydrogeological response of a contaminated site to remediation measures at Hjortsberga, southern Sweden. (15 hp)
602. Barrett, Aodhan, 2020: Major and trace element geochemical analysis of norites in the Hakefjorden Complex to constrain magma source and magma plumbing systems. (45 hp)
603. Lundqvist, Jennie, 2020: ”Man fyller det med information helt enkelt”: en fenomenografisk studie om studenters upplevelse av geologisk tid. (45 hp)
604. Zachén, Gabriel, 2020: Classification of four mesosiderites and implications for their formation. (45 hp)
605. Viðarsdóttir, Halla Margrét, 2020: Assessing the biodiversity crisis whitin the Triassic-Jurassic boundary interval using redox sensitive trace metals and stable carbon isotope geochemistry. (45 hp)
606. Tan, Brian, 2020: Nordvästra Skånes prekambriska geologiska utveckling. (15 hp)
607. Taxopoulou, Maria Eleni, 2020: Metamorphic micro-textures and mineral assemblages in orthogneisses in NW Skåne – how do they correlate with technical properties? (45 hp)
608. Damber, Maja, 2020: A palaeoecological study of the establishment of beech forest in Söderåsen National Park, southern Sweden. (45 hp)
609. Karastergios, Stylianos, 2020: Characterization of mineral parageneses and metamorphic textures in eclogite- to high-pressure granulite-facies marble at Allmenningen, Roan, western Norway. (45 hp)
610. Lindberg Skutsjö, Love, 2021: Geologiska och hydrogeologiska tolkningar av SkyTEM-data från Vombsänkan, Sjöbo kommun, Skåne. (15 hp)
611. Hertzman, Hanna, 2021: Odensjön - A new varved lake sediment record from southern Sweden. (45 hp)
612. Molin, Emmy, 2021: Rare terrestrial vertebrate remains from the Pliensbachian (Lower Jurassic) Hasle Formation on the Island of Bornholm, Denmark. (45 hp)
613. Höjbert, Karl, 2021: Dendrokronologi - en nyckelmetod för att förstå klimat- och miljöförändringar i Jämtland under holocen. (15 hp)
614. Lundgren Sassner, Lykke, 2021: A Method for Evaluating and Mapping Terrestrial Deposition and Preservation Potential- for Palaeostorm Surge Traces. Remote Mapping of the Coast of Scania, Blekinge and Halland, in Southern Sweden, with a Field Study at Dalköpinge Ängar, Trelleborg. (45 hp)
615. Granbom, Johanna, 2021: En detaljerad undersökning av den mellanordoviciska ”furudalkalkstenen” i Dalarna. (15 hp)
616. Greiff, Johannes, 2021: Oolites from the Arabian platform: Archives for the aftermath of the end-Triassic mass extinction. (45 hp)
617. Ekström, Christian, 2021: Rödfärgade

utfällningar i dammanläggningar orsakade av *G. ferruginea* och *L. ochracea* - Problemstatistik och mikrobiella levnadsförutsättningar. (15 hp)

618. Östsjö, Martina, 2021: Geologins betydelse i samhället och ett första steg mot en geopark på Gotland. (15 hp)
619. Westberg, Märta, 2021: The preservation of cells in biomineralized vertebrate tissues of Mesozoic age – examples from a Cretaceous mosasaur (Reptilia, Mosasauridae). (45 hp)
620. Gleisner, Lovisa, 2021: En detaljerad undersökning av kalkstenslager i den mellanordoviciska gullhögenformationen på Billingen i Västergötland. (15 hp)
621. Bonnevier Wallstedt, Ida, 2021: Origin and early evolution of isopods - exploring morphology, ecology and systematics. (15 hp)
622. Selezeneva, Natalia, 2021: Indications for solar storms during the Last Glacial Maximum in the NGRIP ice core. (45 hp)
623. Bakker, Aron, 2021: Geological characterisation of geophysical lineaments as part of the expanded site descriptive model around the planned repository site for high-level nuclear waste, Forsmark, Sweden. (45 hp)
624. Sundberg, Oskar, 2021: Jordlagerföljden i Höjeådalen utifrån nya borrningar. (15 hp)
625. Sartell, Anna, 2021: The igneous complex of Ekmanfjorden, Svalbard: an integrated field, petrological and geochemical study. (45 hp)
626. Juliusson, Oscar, 2021: Implications of ice-bedrock dynamics at Ullstorp, Scania, southern Sweden. (45 hp)
627. Eng, Simon, 2021: Rödslam i svenska kraftdammar - Problematik och potentiella lösningar. (15 hp)
628. Kervall, Hanna, 2021: Feasibility of Enhanced Geothermal Systems in the Precambrian crystalline basement in SW Scania, Sweden. (45 hp)
629. Smith, Thomas, 2022: Assessing the relationship between hypoxia and life on Earth, and implications for the search for habitable exoplanets. (45 hp)
630. Neumann, Daniel, 2022: En mosasaurie (Reptilia, Mosasauridae) av paleocensk ålder? (15 hp)
631. Svensson, David, 2022: Geofysisk och geologisk tolkning av kritskollors utbredning i Ystadsområdet. (15 hp)
632. Allison, Edward, 2022: Avsättning av Black Carbon i sediment från Odensjön, södra Sverige. (15 hp)
633. Jirdén, Elin, 2022: OSL dating of the Mesolithic site Nilsvikdalen 7, Bjorøy, Norway. (45 hp)
634. Wong, Danny, 2022: GIS-analys av effekten vid stormflod/havsnivåhöjning, Morupstrakten, Halland. (15 hp)
635. Lycke, Björn, 2022: Mikroplast i vattenavsatta sediment. (15 hp)
636. Schönherr, Lara, 2022: Grön fältspat i Varbergskomplexet. (15 hp)
637. Funck, Pontus, 2022: Granens ankomst och etablering i Skandinavien under postglacial tid. (15 hp)
638. Brotzen, Olga M., 2022: Geologiska besöksmål och geoparker som plattform för popularisering av geovetenskap. (15 hp)
639. Lodi, Giulia, 2022: A study of carbon, nitrogen, and biogenic silica concentrations in *Cyperus papyrus*, the sedge dominating the permanent swamp of the Okavango Delta, Botswana, Africa. (45 hp)
640. Nilsson, Sebastian, 2022: PFAS- En sammanfattning av ny forskning, med ett fokus på föroreningskällor, provtagning, analysmetoder och saneringsmetoder. (15 hp)
641. Jägfeldt, Hans, 2022: Molnens påverkan på jordens strålningsbalans och klimatsystem. (15 hp)
642. Sundberg, Melissa, 2022: Paleontologiska egenskaper och syreisotopsutveckling i borrkärnan Limhamn-2018: Kopplingar till klimatförändringar under yngre krita. (15 hp)
643. Bjermo, Tim, 2022: A re-investigation of hummocky moraine formed from ice sheet decay using geomorphological and sedimentological evidence in the Vomb area, southern Sweden. (45 hp)

LUNDS UNIVERSITET

Geologiska institutionen
Lunds universitet
Sölvegatan 12, 223 62 Lund